

Tensor Completion by Multi-Rank via Unitary Transformation*

Guang-Jing Song[†] Michael K. Ng[‡] Xiongjun Zhang[§]

January 25, 2022

Abstract: One of the key problems in tensor completion is the number of uniformly random sample entries required for recovery guarantee. The main aim of this paper is to study $n_1 \times n_2 \times n_3$ third-order tensor completion based on transformed tensor singular value decomposition, and provide a bound on the number of required sample entries. Our approach is to make use of the multi-rank of the underlying tensor instead of its tubal rank in the bound. In numerical experiments on synthetic and imaging data sets, we demonstrate the effectiveness of our proposed bound for the number of sample entries. Moreover, our theoretical results are valid to any unitary transformation applied to n_3 -dimension under transformed tensor singular value decomposition.

Keywords: tensor completion, transformed tensor singular value decomposition, sampling sizes, transformed tensor nuclear norm

AMS Subject Classifications 2010: 15A69, 15A83, 90C25

1 Introduction

The problem of recovering an unknown low-rank tensor from a small fraction of its entries is known as the tensor completion problem, and comes up in a wide range of applications, e.g., image processing [13, 25, 41], computer vision [20, 40], and machine learning [30, 31]. The goal of low-rank tensor completion is to recover a tensor with the lowest rank based on observable entries of a given tensor. Given a third-order tensor $\mathcal{M} \in \mathbb{C}^{n_1 \times n_2 \times n_3}$, the low rank tensor completion problem can be expressed as follows:

$$\begin{aligned} \min_{\mathcal{Z}} \text{rank}(\mathcal{Z}) \\ \text{s.t. } \mathcal{P}_\Omega(\mathcal{Z}) = \mathcal{P}_\Omega(\mathcal{M}), \end{aligned} \tag{1}$$

*The research of G.-J. Song was supported in part by the National Natural Science Foundation of China under Grant 12171369 and Key NSF of Shandong Province under Grant ZR2020KA008. The research of M. K. Ng was supported in part by the HKRGC GRF 12300218, 12300519, 17201020, 17300021, and N-HKU769-21. The research of X. Zhang was supported in part by the National Natural Science Foundation of China under Grant Nos. 12171189 and 11801206.

[†]G.-J. Song is with the School of Mathematics and Information Sciences, Weifang University, Weifang 261061, China (e-mail: sgjshu@163.com).

[‡]M. K. Ng is with the Department of Mathematics, The University of Hong Kong, Hong Kong (e-mail: mng@maths.hku.hk).

[§]The Corresponding Author. X. Zhang is with the School of Mathematics and Statistics and Hubei Key Laboratory of Mathematical Sciences, Central China Normal University, Wuhan 430079, China (e-mail: xjzhang@mail.ccnu.edu.cn).

where $\text{rank}(\mathcal{Z})$ denotes the rank of the tensor \mathcal{Z} , Ω is a subset of $\{1, \dots, n_1\} \times \{1, \dots, n_2\} \times \{1, \dots, n_3\}$, and \mathcal{P}_Ω is the projection operator such that the entries in Ω are given while the remaining entries are missing, i.e.,

$$(\mathcal{P}_\Omega(\mathcal{Z}))_{ijk} = \begin{cases} \mathcal{Z}_{ijk}, & \text{if } (i, j, k) \in \Omega, \\ 0, & \text{otherwise.} \end{cases}$$

In particular, if $n_3 = 1$, the tensor completion problem in (1) reduces to the well-known matrix completion problem, which has received a considerable amount of attention in the past decades, see, e.g., [5, 6, 7, 11, 29] and references therein. In the matrix completion problem, a given incoherent $n \times n$ matrix could be recovered with high probability if the uniformly random sample size is of order $O(rn \log(n))$, where r is the rank of the given matrix. This bound has been shown to be optimal, see [7] for detailed discussions.

The main aim of this paper is to study the incoherence conditions of low-rank tensors based on the transformed tensor singular value decomposition (SVD) and provide a lower bound on the number of random sample entries required for exact tensor recovery. Different kinds of tensor ranks setting in model (1) lead to different convex relaxation models and different sample sizes required to exactly recover the original tensor. When the rank in the model (1) is chosen as the Tucker rank [35], Liu et al. [20] proposed to use the sum of the nuclear norms (SNN) of unfolding matrices of a tensor to recover a low Tucker rank tensor. Within the SNN framework, Tomioka et al. [33] proved that a given d -order tensor $\mathcal{X} \in \mathbb{R}^{n \times \dots \times n}$ with Tucker rank (r, \dots, r) can be exactly recovered with high probability if the Gaussian measurements size is of order $O(rn^{d-1})$. Afterwards, Mu et al. [24] showed that $O(rn^{d-1})$ Gaussian measurements are necessary for a reliable recovery by the SNN method. In fact, the degree of freedoms of a tensor $\mathcal{X} \in \mathbb{R}^{n \times \dots \times n}$ with Tucker rank (r_1, \dots, r_d) is $\prod_{i=1}^d r_i + \sum_{i=1}^d (r_i n - r_i^2)$, which is much smaller than $O(rn^{d-1})$. Recently, Yuan et al. [38, 39] showed that an $n \times n \times n$ tensor with Tucker rank (r, r, r) can be exactly recovered with high probability by $O((r^{\frac{1}{2}} n^{\frac{3}{2}} + r^2 n) \log^2(n))$ entries, which have a great improvement compared with the number of sampled sizes required in [24] when n is relatively large. Later, based on a gradient descent algorithm designed on some product smooth manifolds, Xia et al. [37] showed that an $n \times n \times n$ tensor with multi-linear rank (r, r, r) can be reconstructed with high probability by $O(r^{\frac{7}{2}} n^{\frac{3}{2}} \log^{\frac{3}{2}}(n) + r^7 n \log^6(n))$ entries. When the rank in the model (1) is chosen as the CANDECOMP/PARAFAC (CP) rank [18], Mu et.al [24] introduced a square deal method which only uses an individual nuclear norm of a balanced matrix instead of using a combination of all d nuclear norms of unfolding matrices of the tensor. Moreover, they showed that $O(r^{\lfloor \frac{d}{2} \rfloor} n^{\lceil \frac{d}{2} \rceil})$ samples are sufficient to recover a CP rank r tensor with high probability.

Besides, some tensor estimation and recovery problems for the observations with Gaussian measurements were proposed and studied in the literature [1, 3, 21, 27, 34]. For example, Ahmed et al. [1] proposed and studied the tensor regression problem by using low-rank and sparse Tucker decomposition, where a tensor variant of projected gradient descent was proposed and the sample complexity of this algorithm for a d -order tensor $n_1 \times \dots \times n_d$ with Tucker rank (r_1, \dots, r_d) is $O(\bar{r}^d + \bar{s} \bar{r} d \log^2(3 \bar{n} d))$ under the restricted isometry property for sub-Gaussian linear maps. Here $\bar{r} = \max\{r_1, \dots, r_d\}$ and $\bar{n} = \max\{n_1, \dots, n_d\}$ and $\bar{s} = \max\{s_1, \dots, s_d\}$, where s_i is the upper bound of the number of nonzero entries of each column of the i -th factor matrix in the Tucker decomposition. Moreover, Cai et al. [3] showed that the Riemannian gradient algorithm can reconstruct a d -order tensor of size $n \times \dots \times n$ and Tucker rank (r, \dots, r) with high probability from only $O(nr^2 + r^{d+1})$ measurements under the tensor restricted isometry property for Gaussian measurements, where one step of iterative hard thresholding was used for the initialization.

The tubal rank of a third-order tensor was first proposed by Kilmer et al. [16, 17], which is based on tensor-tensor product (t-product). Within the associated algebraic framework of t-product, the tensor SVD was proposed and studied similarly to matrix SVD [17]. For tensor tubal rank minimization, Zhang et al. [42] proved that the tensor tubal nuclear norm (TNN) can be used as a convex relaxation of the tensor tubal rank. Then they showed that an $n \times n \times n$ tensor with tubal rank r can be exactly recovered by $O(rn^2 \log(n^2))$ uniformly sampled entries. However, the TNN is not the convex envelope of the tubal rank of a tensor, which may lead to more sample entries needed to exactly recover the original tensor. In Table 1, we summarize existing results and our contribution for the $n \times n \times n$ tensor completion problem. It is interesting that there are other factors that affect sample sizes requirement such as sampling methods and incoherence conditions. For detailed discussions, the interested readers are referred to [2, 14, 19, 23].

Table 1: Sampling sizes and sampling methods for third-order tensor completion.

Rank Assumption	Sampling Method	Incoherent and Other Conditions	Requirement Sampling Sizes
CP rank r [24]	Gaussian	N/A	$O(rn^2)$
CP rank r [14]	Uniformly Random	Incoherent condition of symmetric tensor	$O(n^{\frac{3}{2}} r^5 \log^4(n))$
Tucker rank (r, r, r) [39]	Uniformly Random	Matrix incoherent condition on model- n unfolding	$O(rn^{\frac{3}{2}} + r^2 n) \log^2(n)$
Tucker rank (r, r, r) [12]	Random	Matrix incoherent condition on model- n unfolding	$O(rn^2 \log^2(n))$
Tucker rank (r, r, r) [24]	Gaussian	N/A	$O(rn^2)$
Tucker rank (r, r, r) [37]	Uniformly Random	Matrix incoherent condition on model- n unfolding	$O(r^{\frac{7}{2}} n^{\frac{3}{2}} \log^{\frac{3}{2}}(n) + r^7 n \log^6(n))$
Tubal rank r [42]	Uniformly Random	Tensor incoherent condition	$O(rn^2 \log(n^2))$
multi-rank (r_1, \dots, r_n) (in this paper)	Uniformly Random	Tensor incoherent condition	$O(\sum_{i=1}^n r_i n \log(n^2))$

In this paper, we mainly study the $n_1 \times n_2 \times n_3$ third-order tensor completion problem based on transformed tensor SVD and transformed tensor nuclear norm (TTNN) [32]. We show that such low-rank tensors can be exactly recovered with high probability when the number of randomly observed entries is of order $O(\sum_{i=1}^{n_3} r_i \max\{n_1, n_2\} \log(\max\{n_1, n_2\} n_3))$, where r_i is the i -th element of the transformed multi-rank of a tensor.

The rest of this paper is organized as follows. In Section 2, the transformed tensor SVD related to an arbitrary unitary transformation is reviewed. In Section 3, we provide the bound on the number of sample entries for tensor completion via any unitary transformation. In Section 4, several synthetic data and imaging data sets are performed to demonstrate that our theoretical result is valid and the performance of the proposed method is better than the existing methods in terms of sample sizes requirement. Some concluding remarks are given in Section 5. Finally, the proofs of auxiliary lemmas supporting our main theorem are provided in the appendix.

2 Transformed Tensor Singular Value Decomposition

First, some notations used throughout this paper are introduced. $\mathbb{N}_{\geq 0}^n$ denotes the nonnegative n -dimensional integers space. We use Φ to denote an arbitrary unitary matrix, i.e., $\Phi\Phi^H = \Phi^H\Phi = I$, where Φ^H is the conjugate transpose of Φ and I is the identity matrix whose dimension should be clear from the context. Tensors are represented by capital Euler script letters, e.g., \mathcal{A} . A tube of a third-order tensor is defined by fixing the first two indices and varying the third [17].

Let $\mathcal{A} \in \mathbb{C}^{n_1 \times n_2 \times n_3}$ be a third-order tensor. \mathcal{A}_{ijk} denotes the (i, j, k) -th entry of \mathcal{A} . We use $\hat{\mathcal{A}}_\Phi$ to denote a third-order tensor obtained as follows:

$$\text{vec}(\hat{\mathcal{A}}_\Phi(i, j, :)) = \Phi(\text{vec}(\mathcal{A}(i, j, :))),$$

where $\text{vec}(\cdot)$ is the vectorization operator from $\mathbb{C}^{1 \times 1 \times n_3}$ to \mathbb{C}^{n_3} and $\mathcal{A}(i, j, :)$ denotes the (i, j) -th tube of \mathcal{A} . For simplicity, we denote $\hat{\mathcal{A}}_\Phi = \Phi[\mathcal{A}]$. In the same fashion, one can also compute \mathcal{A} from $\hat{\mathcal{A}}_\Phi$, i.e., $\mathcal{A} = \Phi^H[\hat{\mathcal{A}}_\Phi]$. A block diagonal matrix can be derived by the frontal slices of \mathcal{A} using the ‘‘blockdiag’’ operator:

$$\text{blockdiag}(\mathcal{A}) := \begin{pmatrix} \mathcal{A}^{(1)} & & & \\ & \mathcal{A}^{(2)} & & \\ & & \ddots & \\ & & & \mathcal{A}^{(n_3)} \end{pmatrix},$$

where $\mathcal{A}^{(i)}$ is the i -th frontal slice of \mathcal{A} , $i = 1, \dots, n_3$. Conversely, the block diagonal matrix $\text{blockdiag}(\mathcal{A})$ can be converted into a tensor via the following ‘‘fold’’ operator:

$$\text{fold}(\text{blockdiag}(\mathcal{A})) := \mathcal{A}.$$

After introducing the tensor notation and terminology, we give the basic definitions about the tensor product, the conjugate transpose of a tensor, the identity tensor and the unitary tensor with respect to the unitary transformation matrix Φ , respectively.

Definition 2.1. [32, Definition 1] The Φ -product of $\mathcal{A} \in \mathbb{C}^{n_1 \times n_2 \times n_3}$ and $\mathcal{B} \in \mathbb{C}^{n_2 \times n_4 \times n_3}$ is a tensor $\mathcal{C} \in \mathbb{C}^{n_1 \times n_4 \times n_3}$, which is given by

$$\mathcal{C} = \mathcal{A} \diamond_\Phi \mathcal{B} = \Phi^H \left[\text{fold} \left(\text{blockdiag}(\hat{\mathcal{A}}_\Phi) \cdot \text{blockdiag}(\hat{\mathcal{B}}_\Phi) \right) \right].$$

Remark 2.1. Kernfeld et al. [15] defined the tensor product between two tensors by using frontal slices products in the transformed domain based on an arbitrary invertible linear transformation. In this paper, we mainly focus on the tensor product based on unitary transformations. Moreover, the relation between Φ -product and tensor product by using fast Fourier transform (FFT) [17] is shown in [32].

Definition 2.2. [32, Definition 2] For any $\mathcal{A} \in \mathbb{C}^{n_1 \times n_2 \times n_3}$, its conjugate transpose with respect to Φ , denoted by $\mathcal{A}^H \in \mathbb{C}^{n_2 \times n_1 \times n_3}$, is defined as

$$\mathcal{A}^H = \Phi^H \left[\text{fold} \left(\text{blockdiag}(\hat{\mathcal{A}}_\Phi)^H \right) \right].$$

Definition 2.3. [15, Proposition 4.1] The identity tensor $\mathcal{I}_\Phi \in \mathbb{C}^{n \times n \times n_3}$ (with respect to Φ) is defined to be a tensor such that $\mathcal{I}_\Phi = \Phi^H[\mathcal{T}]$, where each frontal slice of $\mathcal{T} \in \mathbb{R}^{n \times n \times n_3}$ is the $n \times n$ identity matrix.

Definition 2.4. [15, Definition 5.1] A tensor $\mathcal{Q} \in \mathbb{C}^{n_1 \times n_2 \times n_3}$ is unitary with respect to Φ -product if it satisfies

$$\mathcal{Q}^H \diamond_{\Phi} \mathcal{Q} = \mathcal{Q} \diamond_{\Phi} \mathcal{Q}^H = \mathcal{I}_{\Phi}.$$

In addition, \mathcal{A} is a diagonal tensor if and only if each frontal slice $\mathcal{A}^{(i)}$ of \mathcal{A} is a diagonal matrix. By above definitions, the transformed tensor SVD with respect to Φ can be given as follows.

Theorem 2.2. [15, Theorem 5.1] Suppose that $\mathcal{A} \in \mathbb{C}^{n_1 \times n_2 \times n_3}$. Then \mathcal{A} can be factorized as

$$\mathcal{A} = \mathcal{U} \diamond_{\Phi} \mathcal{S} \diamond_{\Phi} \mathcal{V}^H, \quad (2)$$

where $\mathcal{U} \in \mathbb{C}^{n_1 \times n_1 \times n_3}$, $\mathcal{V} \in \mathbb{C}^{n_2 \times n_2 \times n_3}$ are unitary tensors with respect to Φ -product, and $\mathcal{S} \in \mathbb{C}^{n_1 \times n_2 \times n_3}$ is a diagonal tensor.

Based on the transformed tensor SVD given in Theorem 2.2, the transformed multi-rank and tubal rank of a tensor can be defined as follows.

Definition 2.5. [32, Definition 6] (i) The transformed multi-rank of $\mathcal{A} \in \mathbb{C}^{n_1 \times n_2 \times n_3}$, denoted by $\text{rank}_t(\mathcal{A})$, is a vector $\mathbf{r} \in \mathbb{N}_{\geq 0}^{n_3}$ with its i -th entry being the rank of the i -th frontal slice of $\hat{\mathcal{A}}_{\Phi}$, i.e.,

$$\text{rank}_t(\mathcal{A}_{\Phi}) = \mathbf{r} \quad \text{with} \quad r_i = \text{rank}(\hat{\mathcal{A}}_{\Phi}^{(i)}), \quad i = 1, \dots, n_3.$$

(ii) The transformed tubal rank of $\mathcal{A} \in \mathbb{C}^{n_1 \times n_2 \times n_3}$, denoted by $\text{rank}_{tt}(\mathcal{A})$, is defined as the number of nonzero singular tubes of \mathcal{S} , where \mathcal{S} comes from the transformed tensor SVD of \mathcal{A} , i.e.,

$$\text{rank}_{tt}(\mathcal{A}) = \#\{i : \mathcal{S}(i, i, :) \neq \mathbf{0}\} = \max_i r_i. \quad (3)$$

Remark 2.3. For computational improvement, we will use the skinny transformed tensor SVD throughout this paper unless otherwise stated, which is defined as follows: The skinny transformed tensor SVD of $\mathcal{A} \in \mathbb{C}^{n_1 \times n_2 \times n_3}$ with $\text{rank}_{tt}(\mathcal{A}) = r$ is given as $\mathcal{A} = \mathcal{U} \diamond_{\Phi} \mathcal{S} \diamond_{\Phi} \mathcal{V}^H$, where $\mathcal{U} \in \mathbb{C}^{n_1 \times r \times n_3}$ and $\mathcal{V} \in \mathbb{C}^{n_2 \times r \times n_3}$ satisfying $\mathcal{U}^H \diamond_{\Phi} \mathcal{U} = \mathcal{I}_{\Phi}$, $\mathcal{V}^H \diamond_{\Phi} \mathcal{V} = \mathcal{I}_{\Phi}$, and $\mathcal{S} \in \mathbb{C}^{r \times r \times n_3}$ is a diagonal tensor. Here $\mathcal{I}_{\Phi} \in \mathbb{C}^{r \times r \times n_3}$ is the identity tensor.

The inner product of two tensors $\mathcal{A}, \mathcal{B} \in \mathbb{C}^{n_1 \times n_2 \times n_3}$ related to the unitary transformation Φ is defined as

$$\langle \mathcal{A}, \mathcal{B} \rangle = \sum_{i=1}^{n_3} \langle \mathcal{A}^{(i)}, \mathcal{B}^{(i)} \rangle = \langle \bar{\mathcal{A}}_{\Phi}, \bar{\mathcal{B}}_{\Phi} \rangle, \quad (4)$$

where $\langle \mathcal{A}^{(i)}, \mathcal{B}^{(i)} \rangle$ is the usual inner product of two matrices and $\bar{\mathcal{A}}_{\Phi} = \text{blockdiag}(\mathcal{A}_{\Phi})$. The following fact will be used throughout the paper: For any tensor $\mathcal{A} \in \mathbb{C}^{n_1 \times n_2 \times n_3}$ and $\mathcal{B} \in \mathbb{C}^{n_2 \times n_4 \times n_3}$, one can get that $\mathcal{A} \diamond_{\Phi} \mathcal{B} = \mathcal{C} \Leftrightarrow \bar{\mathcal{A}}_{\Phi} \cdot \bar{\mathcal{B}}_{\Phi} = \bar{\mathcal{C}}_{\Phi}$.

The tensor spectral norm of an arbitrary tensor $\mathcal{A} \in \mathbb{C}^{n_1 \times n_2 \times n_3}$ related to Φ , denoted by $\|\mathcal{A}\|$, can be defined as $\|\mathcal{A}\| = \|\bar{\mathcal{A}}_{\Phi}\|$ [32], i.e., the spectral norm of its block diagonal matrix $\bar{\mathcal{A}}_{\Phi}$ in the transformed domain. Suppose that \mathcal{L} is a tensor operator, its operator norm is defined as $\|\mathcal{L}\|_{\text{op}} = \sup_{\|\mathcal{A}\|_F \leq 1} \|\mathcal{L}(\mathcal{A})\|_F$, where the tensor Frobenius norm of \mathcal{A} is defined as $\|\mathcal{A}\|_F = \sqrt{\sum_{i,j,k} |\mathcal{A}_{ijk}|^2}$. Specifically, if the operator norm can be represented as a tensor \mathcal{L} via Φ -product with \mathcal{A} , we have $\|\mathcal{L}\|_{\text{op}} = \|\mathcal{L}\|$. The tensor infinity norm and the tensor $l_{\infty,2}$ and are defined as

$$\|\mathcal{A}\|_{\infty} = \max_{i,j,k} |\mathcal{A}_{ijk}| \quad \text{and} \quad \|\mathcal{A}\|_{\infty,2} = \max \left\{ \max_i \sqrt{\sum_{b,k} |\mathcal{A}_{ibk}|^2}, \max_j \sqrt{\sum_{a,k} |\mathcal{A}_{ajk}|^2} \right\}.$$

Moreover, the weighted tensor $l_{\infty, w}$ norm with respect to a weighted vector $w = (\alpha_1, \dots, \alpha_{n_3})^H \in \mathbb{R}^{n_3}$ is defined as

$$\|\mathcal{A}\|_{\infty, w} = \max \left\{ \max_i \sqrt{\sum_{b,k} \alpha_k^2 |\mathcal{A}_{ibk}|^2}, \max_j \sqrt{\sum_{a,k} \alpha_k^2 |\mathcal{A}_{ajk}|^2} \right\}, \quad (5)$$

where $\sum_{k=1}^{n_3} \alpha_k^2 = 1$. The aim of this paper is to recover a low transformed multi-rank tensor, which motivates us to introduce the following definition of TTNN.

Definition 2.6. [32, Definition 7] *The transformed tensor nuclear norm of $\mathcal{A} \in \mathbb{C}^{n_1 \times n_2 \times n_3}$, denoted by $\|\mathcal{A}\|_{\text{TTNN}}$, is the sum of nuclear norms of all frontal slices of $\hat{\mathcal{A}}_{\Phi}$, i.e., $\|\mathcal{A}\|_{\text{TTNN}} = \sum_{i=1}^{n_3} \|\hat{\mathcal{A}}_{\Phi}^{(i)}\|_*$.*

Recently, Song et al. [32] showed that the TTNN of a tensor is the convex envelope of the sum of the entries of the transformed multi-rank of a tensor, which is stated in the following.

Lemma 2.4. [32, Lemma 1] *For any tensor $\mathcal{A} \in \mathbb{C}^{n_1 \times n_2 \times n_3}$, let $\text{rank}_{\text{sum}}(\mathcal{A}) = \sum_{i=1}^{n_3} \text{rank}(\hat{\mathcal{A}}_{\Phi}^{(i)})$. Then $\|\mathcal{A}\|_{\text{TTNN}}$ is the convex envelope of $\text{rank}_{\text{sum}}(\mathcal{A})$ on the set $\{\mathcal{A} \mid \|\mathcal{A}\| \leq 1\}$.*

Lemma 2.4 shows that the TTNN is the tightest convex relaxation of the sum of the entries of the transformed multi-rank of the tensor over a unit ball of the tensor spectral norm. That is why the TTNN is effective in studying the tensor recovery theory with transformed multi-rank minimization.

Next we introduce two kinds of tensor basis which will be exploited to derive our main result.

Definition 2.7. (i) *The column basis, denoted as \vec{e}_{ik} , is a tensor of size $n_1 \times 1 \times n_3$ with the $(i, 1, k)$ -th element equaling to 1 and the others equaling to 0.*

(ii) *Denote \check{e}_k as a tensor of size $1 \times 1 \times n_3$ with the $(1, 1, k)$ -th element equaling to 1 and the remaining elements equaling to 0, $(\Phi[\check{e}_k])_j$ as the $(1, 1, j)$ -th element of $\Phi[\check{e}_k]$, $j = 1, \dots, n_3$.*

(iii) *The transformed tube basis, denoted as \check{e}_k , is a tensor of size $1 \times 1 \times n_3$ with the $(1, 1, j)$ -th element of \check{e}_k equaling to $((\Phi[\check{e}_k])_j)^{-1}$, if $(\Phi[\check{e}_k])_j \neq 0$, and 0, otherwise, $j = 1, \dots, n_3$.*

Remark 2.5. *The transformed tube basis \check{e}_k is determined by the unitary transformation matrix and the original tube \check{e}_k , whose detailed formulation can be obtained for a given unitary transformation Φ .*

3 Main Results

In this section, we consider the third-order tensor completion problem, which aims to recover a low transformed multi-rank tensor under some limited observations. Mathematically, the problem can be described as follows:

$$\begin{aligned} \min_{\mathcal{Z}} \quad & \sum_{i=1}^{n_3} \text{rank}(\hat{\mathcal{Z}}_{\Phi}^{(i)}) \\ \text{s.t.} \quad & \mathcal{P}_{\Omega}(\mathcal{Z}) = \mathcal{P}_{\Omega}(\mathcal{M}), \end{aligned}$$

where $\text{rank}(\hat{\mathcal{Z}}_{\Phi}^{(i)})$ is the rank of $\hat{\mathcal{Z}}_{\Phi}^{(i)}$, i.e., the i -th element of the transformed multi-rank of \mathcal{Z} , $i = 1, \dots, n_3$, Ω and $\mathcal{P}_{\Omega}(\mathcal{Z})$ are defined in model (1). Note that the rank minimization problem is NP-hard and the TTNN is the convex envelope of the sum of the entries of the transformed multi-rank of a tensor [32, Lemma 1]. Therefore, we propose to utilize the TTNN as a convex relaxation of the sum of the entries of the transformed multi-rank of a tensor. More precisely speaking, the convex relaxation model is given by

$$\begin{aligned} \min_{\mathcal{Z}} \quad & \|\mathcal{Z}\|_{\text{TTNN}} \\ \text{s.t.} \quad & \mathcal{P}_{\Omega}(\mathcal{Z}) = \mathcal{P}_{\Omega}(\mathcal{M}). \end{aligned} \quad (6)$$

In the following, we need to introduce the tensor incoherence conditions between the underlying tensor \mathcal{Z} and the column basis given in Definition 2.7.

Definition 3.1. Let $\mathcal{Z} \in \mathbb{C}^{n_1 \times n_2 \times n_3}$ with $\text{rank}_t(\mathcal{Z}) = \mathbf{r}$, where $\mathbf{r} = (r_1, \dots, r_{n_3})$. Assume its skinny transformed tensor SVD is $\mathcal{Z} = \mathcal{U} \diamond_{\Phi} \mathcal{S} \diamond_{\Phi} \mathcal{V}^H$. Then \mathcal{Z} is said to satisfy the tensor incoherence conditions, if there exists a parameter $\mu \geq 1$, such that

$$\max_{i=1, \dots, n_1} \max_{k=1, \dots, n_3} \|\mathcal{U}^H \diamond_{\Phi} \vec{e}_{ik}\|_F \leq \sqrt{\frac{\mu \sum_{i=1}^{n_3} r_i}{n_1 n_3}}, \quad (7)$$

$$\max_{j=1, \dots, n_2} \max_{k=1, \dots, n_3} \|\mathcal{V}^H \diamond_{\Phi} \vec{e}_{jk}\|_F \leq \sqrt{\frac{\mu \sum_{i=1}^{n_3} r_i}{n_2 n_3}}, \quad (8)$$

where $\vec{e}_{ik} \in \mathbb{R}^{n_1 \times 1 \times n_3}$ and $\vec{e}_{jk} \in \mathbb{R}^{n_2 \times 1 \times n_3}$ are the column basis.

Denote by T the linear space of tensors

$$T = \{\mathcal{U} \diamond_{\Phi} \mathcal{Y}^H + \mathcal{W} \diamond_{\Phi} \mathcal{V}^H \mid \mathcal{Y} \in \mathbb{C}^{n_2 \times r \times n_3}, \mathcal{W} \in \mathbb{C}^{n_1 \times r \times n_3}\}, \quad (9)$$

and by T^{\perp} its orthogonal complement, where $\mathcal{U} \in \mathbb{C}^{n_1 \times r \times n_3}$ and $\mathcal{V} \in \mathbb{C}^{n_2 \times r \times n_3}$ are column unitary tensors, respectively, i.e., $\mathcal{U}^H \diamond_{\Phi} \mathcal{U} = \mathcal{I}_{\Phi}$, $\mathcal{V}^H \diamond_{\Phi} \mathcal{V} = \mathcal{I}_{\Phi}$. In the light of [40, Proposition B.1], for any $\mathcal{Z} \in \mathbb{C}^{n_1 \times n_2 \times n_3}$, the orthogonal projections onto T and its complementary are given as follows:

$$\begin{aligned} \mathcal{P}_T(\mathcal{Z}) &= \mathcal{U} \diamond_{\Phi} \mathcal{U}^H \diamond_{\Phi} \mathcal{Z} + \mathcal{Z} \diamond_{\Phi} \mathcal{V} \diamond_{\Phi} \mathcal{V}^H - \mathcal{U} \diamond_{\Phi} \mathcal{U}^H \diamond_{\Phi} \mathcal{Z} \diamond_{\Phi} \mathcal{V} \diamond_{\Phi} \mathcal{V}^H, \\ \mathcal{P}_{T^{\perp}}(\mathcal{Z}) &= (\mathcal{I}_{\Phi} - \mathcal{U} \diamond_{\Phi} \mathcal{U}^H) \diamond_{\Phi} \mathcal{Z} \diamond_{\Phi} (\mathcal{I}_{\Phi} - \mathcal{V} \diamond_{\Phi} \mathcal{V}^H). \end{aligned}$$

Denote $n_{(1)} = \max\{n_1, n_2\}$, $n_{(2)} = \min\{n_1, n_2\}$. We can improve the low bound on the number of sampling sizes for tensor completion by using transformed multi-rank instead of using tubal rank, which is stated in the following theorem.

Theorem 3.1. Suppose that $\mathcal{Z} \in \mathbb{C}^{n_1 \times n_2 \times n_3}$ with $\text{rank}_t(\mathcal{Z}) = \mathbf{r}$ and its skinny transformed tensor SVD is $\mathcal{Z} = \mathcal{U} \diamond_{\Phi} \mathcal{S} \diamond_{\Phi} \mathcal{V}^H$, where $\mathbf{r} = (r_1, \dots, r_{n_3})$, $\mathcal{U} \in \mathbb{C}^{n_1 \times r \times n_3}$, $\mathcal{S} \in \mathbb{C}^{r \times r \times n_3}$ and $\mathcal{V} \in \mathbb{C}^{n_2 \times r \times n_3}$ with $\text{rank}_{tt}(\mathcal{Z}) = r$. Suppose that \mathcal{Z} satisfies the tensor incoherence conditions (7)-(8) and the observation set Ω with $|\Omega| = m$ is uniformly distributed among all sets of cardinality, then there exist universal constants $c_0, c_1, c_2 > 0$ such that if

$$m \geq c_0 \mu \sum_{i=1}^{n_3} r_i n_{(1)} \log(n_{(1)} n_3), \quad (10)$$

\mathcal{Z} is the unique minimizer to (6) with probability at least $1 - c_1(n_{(1)} n_3)^{-c_2}$.

Next we compare the number of sample sizes requirement for exact recovery in [42]. Note that the tensor incoherence conditions in [42] are given by

$$\begin{aligned}\max_{i=1,\dots,n_1} \|\mathcal{U}^H \diamond_{\Phi} \vec{e}_{i1}\|_F &\leq \sqrt{\frac{\mu_{old} r}{n_1}}, \\ \max_{j=1,\dots,n_2} \|\mathcal{V}^H \diamond_{\Phi} \vec{e}_{j1}\|_F &\leq \sqrt{\frac{\mu_{old} r}{n_2}},\end{aligned}$$

where r is the tubal rank of the underlying tensor, $\mu_{old} > 0$ is a parameter, Φ is FFT, \vec{e}_{i1} and \vec{e}_{j1} are defined in Definition 2.7. When the number of samples is larger than or equal to $\tilde{c} r n_{(1)} n_3 \log(n_{(1)} n_3)$, the underlying tensor can be recovered exactly [42], where $\tilde{c} > 0$ is a given constant. Neglecting the constants, we know that the bound of sample sizes requirement in Theorem 3.1 is smaller than that of [42] since $\sum_{i=1}^{n_3} r_i$ is smaller than $r n_3$ in general. Especially, when the the vector of the transformed multi-rank \mathbf{r} is sparse, the number of sample sizes requirement given in (10) is much smaller than that in [42] for exact recovery. Moreover, the exact recovery theory in Theorem 3.1 not only holds for FFT but also for any unitary transformation, which is very meaningful in practical applications. Based on Theorem 3.1, for a given data tensor, we can choose a suitable unitary transformation such that the sum of elements of the transformed multi-rank of the underlying tensor is small [32, 41], which can guarantee to derive better results than that by using FFT directly.

To facilitate our proof of the main theorem, we will consider the independent and identically distributed (*i.i.d.*) *Bernoulli-Rademacher model*. More precisely, we assume $\Omega = \{(i, j, k) \mid \delta_{ijk} = 1\}$, where δ_{ijk} are *i.i.d.* Bernoulli variables taking value one with probability $\rho = \frac{m}{n_1 n_2 n_3}$ and zero with probability $1 - \rho$. Such a Bernoulli sampling is denoted by $\Omega \sim \text{Ber}(\rho)$ for short. As a proxy for uniform sampling, the probability of failure under Bernoulli sampling closely approximates the probability of failure under uniform sampling.

Recall the definitions of tensor Frobenius norm and the tensor incoherence conditions given in (7)-(8), we can get the following result easily.

Proposition 3.2. *Let $\mathcal{Z} \in \mathbb{C}^{n_1 \times n_2 \times n_3}$ be an arbitrary tensor with $\text{rank}_t(\mathcal{Z}) = \mathbf{r}$, and T be given as (9). Suppose that the tensor incoherence conditions (7)-(8) are satisfied, then*

$$\|\mathcal{P}_T(\vec{e}_{ik} \diamond_{\Phi} \vec{e}_k \diamond_{\Phi} \vec{e}_{jk}^H)\|_F^2 \leq \frac{2\mu \sum_{i=1}^{n_3} r_i}{n_{(2)} n_3}.$$

Proposition 3.2 plays an important role in the proofs of Lemmas 3.3, 3.4 and 3.5, which can be found in the Appendix.

Lemma 3.3. *Suppose that $\Omega \sim \text{Ber}(\rho)$, where Ω with $|\Omega| = m$ is a set of indices sampled independently and uniformly without replacement, $\rho = \frac{m}{n_1 n_2 n_3}$ and T is given as (9). Then with high probability,*

$$\|\rho^{-1} \mathcal{P}_T \mathcal{P}_{\Omega} \mathcal{P}_T - \mathcal{P}_T\|_{\text{op}} \leq \epsilon, \quad (11)$$

provided that $m \geq C_0 \epsilon^{-2} \mu \sum_{i=1}^{n_3} r_i n_{(1)} \log(n_{(1)} n_3)$ for some numerical constant $C_0 > 0$.

Lemma 3.4. *Suppose that $\mathcal{Z} \in \mathbb{C}^{n_1 \times n_2 \times n_3}$ is a tensor with $\text{rank}_t(\mathcal{Z}) = \mathbf{r}$, Ω, ρ and m are defined in Lemma 3.3. Then for all $c > 1$ and $C_0 > 0$,*

$$\|(\rho^{-1} \mathcal{P}_{\Omega} - \mathcal{I})\mathcal{Z}\| \leq c \left(\frac{\log(n_{(1)} n_3)}{\rho} \|\mathcal{Z}\|_{\infty} + \sqrt{\frac{\log(n_{(1)} n_3)}{\rho}} \|\mathcal{Z}\|_{\infty, w} \right)$$

holds with high probability provided that $m \geq C_0 \epsilon^{-2} \mu \sum_{i=1}^{n_3} r_i n_{(1)} \log(n_{(1)} n_3)$, where \mathcal{I} denotes the identity operator.

Lemma 3.5. *Suppose that $\mathcal{Z} \in \mathbb{C}^{n_1 \times n_2 \times n_3}$ is a tensor with $\text{rank}_t(\mathcal{Z}) = \mathbf{r}$, Ω, ρ and m are defined in Lemma 3.3. Then for some sufficiently large C_0 ,*

$$\|(\rho^{-1} \mathcal{P}_T \mathcal{P}_\Omega - \mathcal{P}_T) \mathcal{Z}\|_{\infty, w} \leq \frac{1}{2} \sqrt{\frac{n_{(1)} n_3}{\mu \sum_{i=1}^{n_3} r_i}} \|\mathcal{Z}\|_\infty + \frac{1}{2} \|\mathcal{Z}\|_{\infty, w} \quad (12)$$

holds with high probability provided that $m \geq C_0 \epsilon^{-2} \mu \sum_{i=1}^{n_3} r_i n_{(1)} \log(n_{(1)} n_3)$.

The proofs of the three lemmas are left to the appendix. Lemma 3.4 establishes an upper bound of the tensor spectral norm of $(\rho^{-1} \mathcal{P}_\Omega - \mathcal{I}) \mathcal{Z}$ in terms of $\|\mathcal{Z}\|_\infty$ and $\|\mathcal{Z}\|_{\infty, w}$, which is tighter than the existing result given by $\|\mathcal{Z}\|_\infty$ and $\|\mathcal{Z}\|_{\infty, 2}$. The weights in $\|\mathcal{Z}\|_{\infty, w}$ are determined by the unitary transformation, which guarantee the upper bound of $\|(\rho^{-1} \mathcal{P}_\Omega - \mathcal{I}) \mathcal{Z}\|$ to be smaller. Lemma 3.5 shows that the $l_{\infty, w}$ norm of $(\rho^{-1} \mathcal{P}_T \mathcal{P}_\Omega - \mathcal{P}_T) \mathcal{Z}$ can be dominated by $\|\mathcal{Z}\|_{\infty, w}$ and $\|\mathcal{Z}\|_\infty$. Moreover, Lemmas C1 and C2 in [42] can be seen as special cases of Lemmas 3.4 and 3.5, respectively, if the transformation is chosen as FFT.

Lemma 3.6. [42, Lemma 4.1] *Suppose that $\|\rho^{-1} \mathcal{P}_T \mathcal{P}_\Omega \mathcal{P}_T - \mathcal{P}_T\|_{\text{op}} \leq \frac{1}{2}$. Then for any $\mathcal{Z} \in \mathbb{C}^{n_1 \times n_2 \times n_3}$ such that $\mathcal{P}_\Omega(\mathcal{Z}) = 0$, the following inequality*

$$\frac{1}{2} \|\mathcal{P}_{T^\perp}(\mathcal{Z})\|_{\text{TTNN}} > \frac{1}{4n_{(1)} n_3} \|\mathcal{P}_T(\mathcal{Z})\|_F$$

holds with high probability.

With the tools in hand we can list the proof of Theorem 3.1 in detail.

Proof of Theorem 3.1. The high level road map of the proof is a standard one just as shown in [4]: by convex analysis, to show \mathcal{Z} is the unique optimal solution to the problem (6), it is sufficient to find a dual certificate \mathcal{Y} satisfying several subgradient type conditions. In our case, we need to find a tensor $\mathcal{Y} = \mathcal{P}_\Omega(\mathcal{Y})$ such that

$$\|\mathcal{P}_T(\mathcal{Y}) - \mathcal{U} \diamond_{\Phi} \mathcal{V}^H\|_F \leq \frac{1}{4n_{(1)} n_3^2}, \quad (13)$$

$$\|\mathcal{P}_{T^\perp}(\mathcal{Y})\| \leq \frac{1}{2}. \quad (14)$$

It follows from (14) that we need to estimate the tensor spectral norm $\|\mathcal{P}_{T^\perp}(\mathcal{Y})\|$. Similar to matrix cases [4], we can use the tensor infinite norm to establish the upper bound of $\|\mathcal{P}_{T^\perp}(\mathcal{Y})\|$. However, if $\|\mathcal{Y}\|_\infty$ is applied, then it will ultimately link to $\|\mathcal{U} \diamond_{\Phi} \mathcal{V}^H\|_\infty$ and lead to the joint incoherence condition. In order to avoid applying the joint incoherence condition, $\|\mathcal{Y}\|_{\infty, 2}$ is used in [8] and [42] to compute the upper bound of $\|\mathcal{Y}\|$ for the matrix and tensor cases, respectively. It follows from [8] and [42] that a lower upper bound can be derived by using $\|\mathcal{Y}\|_{\infty, 2}$. However, the upper bound derived by $\|\mathcal{Y}\|_{\infty, 2}$ can be relaxed further for an arbitrary unitary transformation. Here, we derive a new upper bound of $\|\mathcal{P}_{T^\perp}(\mathcal{Y})\|$ by using the $l_{\infty, w}$ norm $\|\mathcal{Y}\|_{\infty, w}$ as defined in (5). Note that $\|\mathcal{Y}\|_{\infty, w}$ is not larger than $\|\mathcal{Y}\|_{\infty, 2}$ for any tensor \mathcal{Y} , which leads to a tighter upper bound of $\|\mathcal{Y}\|$.

We now return to the proof Theorem 3.1 in detail. We apply the Golfing Scheme method introduced by Gross [11] and modified by Candès et al. [4] to construct a dual tensor \mathcal{Y} supported by Ω^c iteratively. Similar to the proof of [42, Theorem 3.1], we consider the set $\Omega^c \sim \text{Ber}(1 - \rho)$ as a union of sets of support Ω_j , i.e., $\Omega^c = \bigcup_{j=1}^p \Omega_j$, where

$\Omega_j \sim \text{Ber}(q)$, which implies $q \geq C_0\rho/\log(n_{(1)}n_3)$. Hence we have $\rho = (1 - q)^p$, where $p = \lfloor 5 \log(n_{(1)}n_3) + 1 \rfloor$. Denote

$$\mathcal{Y} = \sum_{j=1}^p \frac{1}{q} \mathcal{P}_{\Omega_j}(\mathcal{Z}_{j-1}), \text{ with } \mathcal{Z}_j = \left(\mathcal{P}_T - \frac{1}{q} \mathcal{P}_T \mathcal{P}_{\Omega_j} \mathcal{P}_T \right) \mathcal{Z}_{j-1}, \mathcal{Z}_0 = \mathcal{P}_T(\mathcal{U} \diamond_{\Phi} \mathcal{V}^H). \quad (15)$$

In the following we will show that \mathcal{Y} defined in (15) satisfies the conditions (13) and (14).

For (13). Set $\mathcal{D}_k := \mathcal{U} \diamond_{\Phi} \mathcal{V}^H - \mathcal{P}_T(\mathcal{Z}_k)$ for $k = 0, \dots, p$. By the definition of \mathcal{Z}_k , we have $\mathcal{D}_0 = \mathcal{U} \diamond_{\Phi} \mathcal{V}^H$ and

$$\mathcal{D}_k = (\mathcal{P}_T - \mathcal{P}_T \mathcal{P}_{\Omega_k} \mathcal{P}_T) \mathcal{D}_{k-1}, \quad k = 1, \dots, p. \quad (16)$$

Note that Ω_k is independent of \mathcal{D}_{k-1} and $q \geq c_0\mu \sum r_i \log(n_{(1)}n_3)/(n_{(1)}n_3)$. For each k , replacing Ω by Ω_k , then by Lemma 3.3, we have

$$\|\mathcal{D}_k\|_F \leq \|\mathcal{P}_T - \mathcal{P}_T \mathcal{P}_{\Omega_k} \mathcal{P}_T\| \|\mathcal{D}_{k-1}\|_F \leq \frac{1}{2} \|\mathcal{D}_{k-1}\|_F.$$

As a consequence, one can obtain that

$$\|\mathcal{P}_T(\mathcal{Y}) - \mathcal{U} \diamond_{\Phi} \mathcal{V}^H\|_F = \|\mathcal{D}_p\|_F \leq \left(\frac{1}{2}\right)^p \|\mathcal{U} \diamond_{\Phi} \mathcal{V}^H\|_F \leq \frac{1}{4(n_{(1)}n_3)^2} \sqrt{r} \leq \frac{1}{4n_{(1)}n_3^2}.$$

For (14). Note that $\mathcal{Y} = \sum_{k=1}^p \mathcal{P}_{\Omega_k} \mathcal{P}_T(\mathcal{D}_{k-1})$, thus

$$\|\mathcal{P}_{T^\perp}(\mathcal{Y})\| \leq \sum_{k=1}^p \|\mathcal{P}_{T^\perp}(\mathcal{P}_{\Omega_k} \mathcal{P}_T - \mathcal{P}_T)(\mathcal{D}_{k-1})\| \leq \sum_{k=1}^p \|(\mathcal{P}_{\Omega_k} - \mathcal{I}) \mathcal{P}_T(\mathcal{D}_{k-1})\|. \quad (17)$$

Applying Lemma 3.4 with Ω replaced by Ω_k to each summand of (17) yields

$$\begin{aligned} \|\mathcal{P}_{T^\perp}(\mathcal{Y})\| &\leq c \sum_{k=1}^p \left(\frac{\log(n_{(1)}n_3)}{q} \|\mathcal{D}_{k-1}\|_\infty + \sqrt{\frac{\log(n_{(1)}n_3)}{q}} \|\mathcal{D}_{k-1}\|_{\infty, w} \right) \\ &\leq \frac{c}{\sqrt{c_0}} \sum_{k=1}^p \left(\frac{n_{(1)}n_3}{\mu \sum r_i} \|\mathcal{D}_{k-1}\|_\infty + \sqrt{\frac{n_{(1)}n_3}{\mu \sum r_i}} \|\mathcal{D}_{k-1}\|_{\infty, w} \right). \end{aligned} \quad (18)$$

Using (16), and applying Lemma 3.3 with Ω replaced by Ω_k , we can get

$$\|\mathcal{D}_{k-1}\|_\infty = \|(\mathcal{P}_{T^\perp}(\mathcal{P}_{\Omega_{k-1}} \mathcal{P}_T - \mathcal{P}_T) \cdots \mathcal{P}_{T^\perp}(\mathcal{P}_{\Omega_1} \mathcal{P}_T - \mathcal{P}_T)) \mathcal{D}_0\|_\infty \leq \frac{1}{2^k} \|\mathcal{U} \diamond_{\Phi} \mathcal{V}^H\|_\infty.$$

It follows from Lemma 3.5 that

$$\|\mathcal{D}_{k-1}\|_{\infty, w} = \|(\mathcal{P}_T - \mathcal{P}_T \mathcal{P}_{\Omega_{k-1}} \mathcal{P}_T) \mathcal{D}_{k-2}\|_{\infty, w} \leq \frac{1}{2} \sqrt{\frac{n_{(1)}n_3}{\mu \sum r_i}} \|\mathcal{D}_{k-2}\|_\infty + \frac{1}{2} \|\mathcal{D}_{k-2}\|_{\infty, w}$$

holds with high probability. Moreover, it follows from (16) that

$$\|\mathcal{D}_{k-1}\|_{\infty, w} \leq \frac{k}{2^{k-1}} \sqrt{\frac{n_{(1)}n_3}{\mu \sum r_i}} \|\mathcal{U} \diamond_{\Phi} \mathcal{V}^H\|_\infty + \frac{1}{2^{k-1}} \|\mathcal{U} \diamond_{\Phi} \mathcal{V}^H\|_{\infty, w}.$$

Taking them back to (18) yields

$$\begin{aligned} & \|\mathcal{P}_{T^\perp}(\mathcal{Y})\| \\ & \leq \frac{c}{\sqrt{c_0}} \frac{n_{(1)}n_3}{\mu \sum r_i} \|\mathcal{U} \diamond_{\Phi} \mathcal{V}^H\|_{\infty} \sum_{k=1}^p (k+1) \left(\frac{1}{2}\right)^{k-1} \end{aligned} \quad (19)$$

$$\begin{aligned} & + \frac{c}{\sqrt{c_0}} \sqrt{\frac{n_{(1)}n_3}{\mu \sum r_i}} \|\mathcal{U} \diamond_{\Phi} \mathcal{V}^H\|_{\infty, w} \sum_{k=1}^p \left(\frac{1}{2}\right)^{k-1} \\ & \leq \frac{6c}{\sqrt{c_0}} \frac{n_{(1)}n_3}{\mu \sum r_i} \|\mathcal{U} \diamond_{\Phi} \mathcal{V}^H\|_{\infty} + \frac{2c}{\sqrt{c_0}} \sqrt{\frac{n_{(1)}n_3}{\mu \sum r_i}} \|\mathcal{U} \diamond_{\Phi} \mathcal{V}^H\|_{\infty, w}. \end{aligned} \quad (20)$$

By the incoherence conditions given in (7)-(8), we can get

$$\|\mathcal{U} \diamond_{\Phi} \mathcal{V}^H\|_{\infty} \leq \max_{i,j,k} \|\mathcal{U} \diamond_{\Phi} \vec{e}_{ik}\|_F \|\mathcal{V}^H \diamond_{\Phi} \vec{e}_{ik}\|_F \leq \frac{\mu \sum r_i}{n_{(1)}n_3}, \quad (21)$$

$$\|\mathcal{U} \diamond_{\Phi} \mathcal{V}^H\|_{\infty, w} \leq \max \left\{ \max_{i,k} \|\mathcal{U} \diamond_{\Phi} \mathcal{V}^H \diamond_{\Phi} \vec{e}_{ik}\|_F, \max_{j,k} \|\vec{e}_{jk}^H \diamond_{\Phi} \mathcal{U} \diamond_{\Phi} \mathcal{V}^H\|_F \right\} \leq \sqrt{\frac{\mu \sum r_i}{n_{(1)}n_3}}. \quad (22)$$

Plugging (21) and (22) into (20), we obtain that

$$\|\mathcal{P}_{T^\perp}(\mathcal{Y})\| \leq \frac{6c}{\sqrt{c_0}} + \frac{2c}{\sqrt{c_0}} \leq \frac{1}{2}$$

provided c_0 is sufficiently large.

Moreover, for any tensor $\mathcal{W} \in \{\mathcal{W} \in \mathbb{C}^{n_1 \times n_1 \times n_3} | \mathcal{P}_{\Omega}(\mathcal{W}) = 0\}$, denote the skinny transformed tensor SVD of $\mathcal{P}_{T^\perp}(\mathcal{W})$ by

$$\mathcal{P}_{T^\perp}(\mathcal{W}) = \mathcal{U}_{\perp} \diamond_{\Phi} \mathcal{S}_{\perp} \diamond_{\Phi} \mathcal{V}_{\perp}^H.$$

Since $\bar{\mathcal{U}}_{\Phi}^H \cdot (\bar{\mathcal{U}}_{\perp})_{\Phi} = \mathbf{0}$ and $\bar{\mathcal{V}}_{\Phi}^H \cdot (\bar{\mathcal{V}}_{\perp})_{\Phi} = \mathbf{0}$, we have

$$\|\mathcal{U} \diamond_{\Phi} \mathcal{V}^H + \mathcal{U}_{\perp} \diamond_{\Phi} \mathcal{V}_{\perp}^H\| = \|\bar{\mathcal{U}}_{\Phi} \cdot \bar{\mathcal{V}}_{\Phi}^H + (\bar{\mathcal{U}}_{\perp})_{\Phi} \cdot ((\bar{\mathcal{V}}_{\perp})_{\Phi})^H\| = 1.$$

Thus, we get that

$$\begin{aligned} \|\mathcal{Z} + \mathcal{W}\|_{\text{TTNN}} & \geq \langle \mathcal{U} \diamond_{\Phi} \mathcal{V}^H + \mathcal{U}_{\perp} \diamond_{\Phi} \mathcal{V}_{\perp}^H, \mathcal{Z} + \mathcal{W} \rangle \\ & = \langle \mathcal{U} \diamond_{\Phi} \mathcal{V}^H, \mathcal{Z} \rangle + \langle \mathcal{U}_{\perp} \diamond_{\Phi} \mathcal{V}_{\perp}^H, \mathcal{P}_{T^\perp}(\mathcal{W}) \rangle + \langle \mathcal{U} \diamond_{\Phi} \mathcal{V}^H, \mathcal{W} \rangle \\ & = \|\mathcal{Z}\|_{\text{TTNN}} + \|\mathcal{P}_{T^\perp}(\mathcal{W})\|_{\text{TTNN}} + \langle \mathcal{U} \diamond_{\Phi} \mathcal{V}^H, \mathcal{W} \rangle \\ & \geq \|\mathcal{Z}\|_{\text{TTNN}} + \|\mathcal{P}_{T^\perp}(\mathcal{W})\|_{\text{TTNN}} - |\langle \mathcal{Y} - \mathcal{U} \diamond_{\Phi} \mathcal{V}^H, \mathcal{W} \rangle - \langle \mathcal{Y}, \mathcal{W} \rangle| \\ & \geq \|\mathcal{Z}\|_{\text{TTNN}} + \|\mathcal{P}_{T^\perp}(\mathcal{W})\|_{\text{TTNN}} - \|\mathcal{P}_{T^\perp}(\mathcal{Y})\| \|\mathcal{P}_{T^\perp}(\mathcal{W})\|_{\text{TTNN}} \\ & \quad - \|\mathcal{P}_T(\mathcal{Y}) - \mathcal{U} \diamond_{\Phi} \mathcal{V}^H\|_F \|\mathcal{P}_T(\mathcal{W})\|_F \\ & \geq \|\mathcal{Z}\|_{\text{TTNN}} + \frac{1}{2} \|\mathcal{P}_{T^\perp}(\mathcal{W})\|_{\text{TTNN}} - \frac{1}{4n_{(1)}n_3} \|\mathcal{P}_T(\mathcal{W})\|_F. \end{aligned} \quad (23)$$

Thus, it follows from Lemma 3.6 that $\|\mathcal{Z} + \mathcal{W}\|_{\text{TTNN}} > \|\mathcal{Z}\|_{\text{TTNN}}$ holds for any \mathcal{W} with $\mathcal{P}_{\Omega}(\mathcal{W}) = 0$. As a consequence, \mathcal{Z} is the unique minimizer to (6). This completes the proof. \square

In the next section, we demonstrate that the theoretical results can be obtained under valid incoherence conditions and the tensor completion performance of the proposed method is better than that of other testing methods.

4 Experimental Results

In this section, numerical examples are presented to demonstrate the effectiveness of the proposed model. All numerical experiments are obtained from a desktop computer running on 64-bit Windows Operating System having 8 cores with Intel(R) Core(TM) i7-6700 CPU at 3.40GHz and 20 GB memory.

Firstly, we employ an alternating direction method of multipliers (ADMM) [9, 10] to solve problem (6). Let $\mathcal{Z} = \mathcal{Y}$. Then problem (6) can be rewritten as

$$\begin{aligned} \min_{\mathcal{Z}} \quad & \|\mathcal{Z}\|_{\text{TTNN}} \\ \text{s.t.} \quad & \mathcal{Z} = \mathcal{Y}, \mathcal{P}_{\Omega}(\mathcal{Y}) = \mathcal{P}_{\Omega}(\mathcal{M}). \end{aligned} \quad (24)$$

The augmented Lagrangian function associated with (24) is defined as

$$L(\mathcal{Z}, \mathcal{Y}, \mathcal{X}) := \|\mathcal{Z}\|_{\text{TTNN}} - \langle \mathcal{X}, \mathcal{Z} - \mathcal{Y} \rangle + \frac{\beta}{2} \|\mathcal{Z} - \mathcal{Y}\|_F^2,$$

where $\mathcal{X} \in \mathbb{C}^{n_1 \times n_2 \times n_3}$ is the Lagrangian multiplier and $\beta > 0$ is the penalty parameter. The ADMM iteration system is given as follows:

$$\mathcal{Z}^{k+1} = \arg \min_{\mathcal{Z}} \left\{ L(\mathcal{Z}, \mathcal{Y}^k, \mathcal{X}^k) \right\}, \quad (25)$$

$$\mathcal{Y}^{k+1} = \arg \min_{\mathcal{Y}} \left\{ L(\mathcal{Z}^{k+1}, \mathcal{Y}, \mathcal{X}^k) : \mathcal{P}_{\Omega}(\mathcal{Y}) = \mathcal{P}_{\Omega}(\mathcal{M}) \right\}, \quad (26)$$

$$\mathcal{X}^{k+1} = \mathcal{X}^k - \gamma\beta (\mathcal{Z}^{k+1} - \mathcal{Y}^{k+1}), \quad (27)$$

where $\gamma \in (0, \frac{1+\sqrt{5}}{2})$ is the dual steplength. It follows from [32, Theorem 3] that the optimal solution with respect to \mathcal{Z} in (25) is given by

$$\mathcal{Z}^{k+1} = \mathcal{U} \diamond_{\Phi} \mathcal{S}_{\beta} \diamond_{\Phi} \mathcal{V}^H, \quad (28)$$

where $\mathcal{Y}^k + \frac{1}{\beta} \mathcal{X}^k = \mathcal{U} \diamond_{\Phi} \mathcal{S} \diamond_{\Phi} \mathcal{V}^H$, $\mathcal{S}_{\beta} = \Phi^H[\hat{\mathcal{S}}_{\beta}]$, and $\hat{\mathcal{S}}_{\beta} = \max\{\hat{\mathcal{S}}_{\Phi} - \frac{1}{\beta}, 0\}$.

The optimal solution with respect to \mathcal{Y} in (26) is given by

$$\mathcal{Y}^{k+1} = \mathcal{P}_{\bar{\Omega}} \left(\mathcal{Z}^{k+1} - \frac{1}{\beta} \mathcal{X}^k \right) + \mathcal{P}_{\Omega}(\mathcal{M}), \quad (29)$$

where $\bar{\Omega}$ denotes the complementary set of Ω on $\{1, \dots, n_1\} \times \{1, \dots, n_2\} \times \{1, \dots, n_3\}$. The detailed description of ADMM for solving (24) is given in Algorithm 1.

Algorithm 1 Alternating direction method of multipliers for solving (24)

Step 0. Let $\tau \in (0, (1+\sqrt{5})/2)$, $\beta > 0$ be given constants. Given $\mathcal{Y}^0, \mathcal{X}^0$. For $k = 0, 1, 2, \dots$, perform the following steps:

Step 1. Compute \mathcal{Z}^{k+1} by (28).

Step 2. Compute \mathcal{Y}^{k+1} via (29).

Step 3. Compute \mathcal{X}^{k+1} by (27).

The convergence of a two-block ADMM for solving convex optimization problems has been established in [9, Theorem B.1] and the convergence of Algorithm 1 can be derived from this theorem easily. We omit the details here for the sake of brevity.

The Karush-Kuhn-Tucker (KKT) conditions associated with problem (24) are given as follows:

$$\begin{cases} 0 \in \partial\|\mathcal{Z}\|_{\text{TTNN}} - \mathcal{X}, \\ \mathcal{Z} = \mathcal{Y}, \mathcal{P}_\Omega(\mathcal{Y}) = \mathcal{P}_\Omega(\mathcal{M}), \end{cases} \quad (30)$$

where $\partial\|\mathcal{Z}\|_{\text{TTNN}}$ denotes the subdifferential of TTNN at \mathcal{Z} . Based on the KKT conditions in (30), we adopt the following relative residual to measure the accuracy of a computed solution in the numerical experiments:

$$\eta := \max\{\eta_x, \eta_y\},$$

where

$$\eta_x = \frac{\|\mathcal{Z} - \text{Prox}_{\|\cdot\|_{\text{TTNN}}}(\mathcal{X} + \mathcal{Z})\|_F}{1 + \|\mathcal{Z}\|_F + \|\mathcal{X}\|_F}, \quad \eta_y = \frac{\|\mathcal{Z} - \mathcal{Y}\|_F}{1 + \|\mathcal{Z}\|_F + \|\mathcal{Y}\|_F}.$$

Here $\text{Prox}_f(y) := \arg \min_x \{f(x) + \frac{1}{2}\|x - y\|^2\}$. In the practical implementation, Algorithm 1 will be terminated if $\eta \leq 10^{-3}$ or the maximum number of iterations exceeds 600. We set $\gamma = 1.618$ for the convergence of ADMM [9] in all experiments. Since the penalty parameter β is not too sensitive to the recovered results, we set $\beta = 0.05$ in the following experiments. The relative error (Rel) is defined by

$$\text{Rel} := \frac{\|\mathcal{Z}_{est} - \mathcal{Z}\|_F}{\|\mathcal{Z}\|_F},$$

where \mathcal{Z}_{est} is the estimated tensor and \mathcal{Z} is the ground-truth tensor. To evaluate the performance of the proposed method for real-world tensors, the peak signal-to-noise ratio (PSNR) is used to measure the quality of the estimated tensor, which is defined as follows:

$$\text{PSNR} := 10 \log_{10} \frac{n_1 n_2 n_3 (\mathcal{Z}_{\max} - \mathcal{Z}_{\min})^2}{\|\mathcal{Z}_{est} - \mathcal{Z}\|_F^2},$$

where \mathcal{Z}_{\max} and \mathcal{Z}_{\min} denote the maximum and minimum entries of \mathcal{Z} , respectively. The structural similarity (SSIM) index [36] is used to measure the quality of the recovered images:

$$\text{SSIM} := \frac{(2\mu_x\mu_y + c_1)(2\sigma_{xy} + c_2)}{(\mu_x^2 + \mu_y^2 + c_1)(\sigma_x^2 + \sigma_y^2 + c_2)},$$

where μ_x, σ_x are the mean intensities and standard deviation of the original image, respectively, μ_y, σ_y denote the mean intensities and standard deviation of the recovered images, respectively, σ_{xy} denotes the covariance of the original and recovered images, and $c_1, c_2 > 0$ are constants. For the real-world tensor data, the SSIM is used to denote the average SSIM values of all images.

4.1 Transformations of tensor SVD

In this subsection, we use three kinds of transformations in the Φ -product and transformed tensor SVD. The first two transformations are FFT (t-SVD (FFT)) and discrete cosine transform (t-SVD (DCT)). The third one is based on given data to construct a unitary transform matrix [26, 32, 41]. Note that we unfold \mathcal{Z} into a matrix Z along the third-dimension (called t-SVD (data)) and take the SVD of the unfolding matrix $Z = U\Sigma V^H$. Suppose that $\text{rank}(Z) = r$. It is interesting to observe that U^H is the optimal transformation to obtain a low rank approximation of Z :

$$\min_{\Phi, B} \|\Phi Z - B\|_F^2 \quad \text{s.t.} \quad \text{rank}(B) = r, \quad \Phi^H \Phi = \Phi \Phi^H = I.$$

It has been demonstrated that the chosen unitary transformation U^H is very effective for the tensor completion problems in the literature, e.g., [26, 32, 41]. In practice, the estimator of \mathcal{Z} obtained by t-SVD (DCT) can be used to generate Φ for tensor completion.

Now we give the computational cost of TTNN based on the three transformations for any $n_1 \times n_2 \times n_3$ tensor, which is the main cost of Algorithm 1. Suppose that $n_2 \leq n_1$. The computational cost of TTNN is given as follows:

- The application of FFT or DCT to a tube (n_3 -vector) is of $O(n_3 \log(n_3))$ operations. There are $n_1 n_2$ tubes in an $n_1 \times n_2 \times n_3$ tensor. In the transformed tensor SVD based on FFT or DCT, we need to compute n_3 n_1 -by- n_2 SVDs in the transformed domain and then the cost is $O(n_1 n_2^2 n_3)$ for these matrices. Hence, the total cost of TTNN based on FFT or DCT is of $O(n_1 n_2 n_3 \log(n_3) + n_1 n_2^2 n_3)$ operations.
- The application of a unitary transformation (n_3 -by- n_3) to an n_3 -vector is of $O(n_3^2)$ operations. And there are still n_3 n_1 -by- n_2 SVDs to be calculated in the transformed domain. Therefore, the total cost of computing the TTNN based on the given data is of $O(n_1 n_2 n_3^2 + n_1 n_2^2 n_3)$ operations.

4.2 Recovery Results

In this subsection, we show the recovery results to demonstrate the performance of our analysis for synthetic data and real imaging data sets.

4.2.1 Synthetic Data

For the synthetic data, the random tensors are generated as follows: $\mathcal{Z} = \mathcal{A} \diamond_{\Phi} \mathcal{B} \in \mathbb{C}^{n_1 \times n_2 \times n_3}$ with different transformed multi-rank \mathbf{r} , where $\hat{\mathcal{A}}_{\Phi}^{(i)}$ and $\hat{\mathcal{B}}_{\Phi}^{(i)}$ are generated by MATLAB commands `randn(n_1, r_i)` and `randn(n_2, r_i)`, and r_i is the i -th element of the transformed multi-rank \mathbf{r} . Here Φ denotes FFT, DCT, and an orthogonal matrix generated by the SVD of the unfolding matrix of \mathcal{Z} along the third-dimension, see Section 4.1.

In Figures 1 and 2, we show the actual number of sample sizes for exact recovery and the theoretical bounds of sample sizes requirements in Theorem 3.1:

$$m \geq \text{constant}_1 \sum_{i=1}^n r_i n \log(n^2) \quad (31)$$

and the results in [42]:

$$m \geq \text{constant}_2 r n^2 \log(n^2) \quad (32)$$

for the $n \times n \times n$ tensor with the fixed sum of the transformed multi-rank and fixed transformed tubal rank by using t-SVD (FFT), t-SVD (DCT), and t-SVD (data). In the randomly generated tensor, we set (i) $\max_{1 \leq i \leq n} r_i = 10$ (the transformed tubal rank is 10) and $\sum_{i=1}^n r_i = 200$; and (ii) $\max_{1 \leq i \leq n} r_i = 20$ (the transformed tubal rank is 20) and $\sum_{i=1}^n r_i = 300$.

In Figures 1 and 2, we test different values of n (from 60 to 200 with the increment size being 20). The exact recovery means that five trials are tested and all of the relative errors are less than or equal to 10^{-2} in the experiments. We test constant_1 , $\text{constant}_2 = 0.5$ or 1 in the right hand sides of (31) and (32) respectively to check how the theoretical bounds of sample sizes match with the actual number of samples for different values of n . It can be seen from Figures 1 and 2 that the curve $\sum_{i=1}^n r_i n \log(n^2)$ based on the proposed bound with $\text{constant}_1 = 1$ is close to the curve for the number of samples required by using t-SVD (FFT),

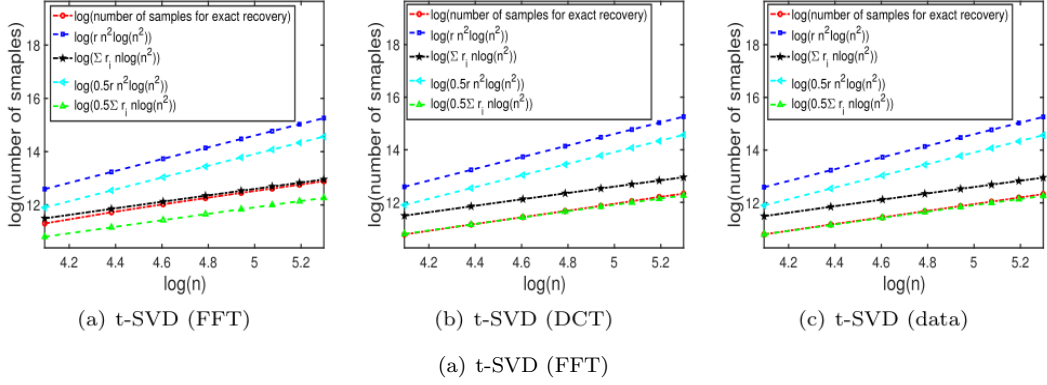


Figure 1: The number of samples of exact recovery, the sample sizes required by the right hand sides of (31) and (32) for different values of n with $\sum_{i=1}^n r_i = 200$.

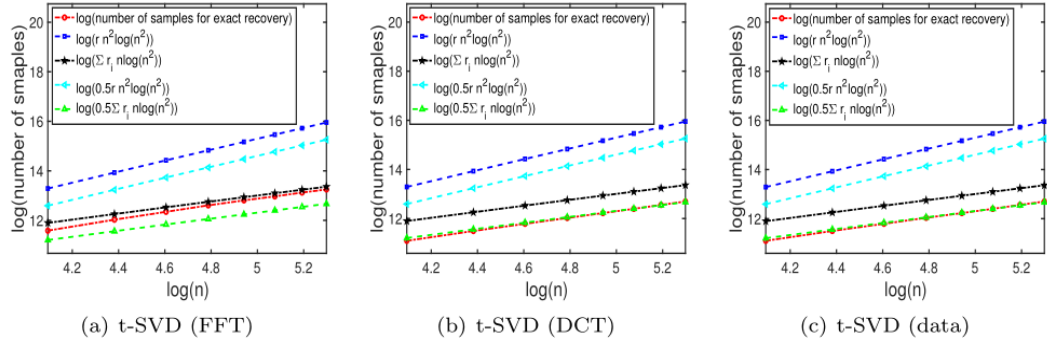


Figure 2: The number of samples of exact recovery, the sample sizes required by the right hand sides of (31) and (32) for different values of n with $\sum_{i=1}^n r_i = 300$.

and the curves $0.5 \sum_{i=1}^n r_i n \log(n^2)$ based on the proposed bound with constant₁ = 0.5 is close to the curves for the number of samples required by using t-SVD (DCT) and t-SVD (data). Note that the corresponding slope of these lines in Figures 1 and 2 is equal to 1 derived by the n term. In contrast, the curves constant₂ $r n^2 \log(n^2)$ based on the results in [42] do not fit the curves for the number of samples required by using t-SVD (FFT), t-SVD (DCT) and t-SVD (data), see the curves with constant₂ = 0.5, 1 in Figures 1 and 2. The main reason is that the corresponding slope of the lines in Figures 1 and 2 is equal to 2 derived by the n^2 term. According to Figures 1 and 2, we find that the theoretical bounds of sample sizes requirements in Theorem 3.1 match with the actual number of sample sizes for recovery.

4.2.2 Hyperspectral Images

In this subsection, two hyperspectral data sets (Samson ($95 \times 95 \times 156$) and Japser Ridge ($100 \times 100 \times 198$) [43]) are used to demonstrate the required number of samples for tensor recovery by the proposed bound. For Samson data, n_1 and n_2 are equal to 95 and n_3 is equal to 156. For Japser Ridge data, n_1 and n_2 are equal to 100 and n_3 is equal to 198.

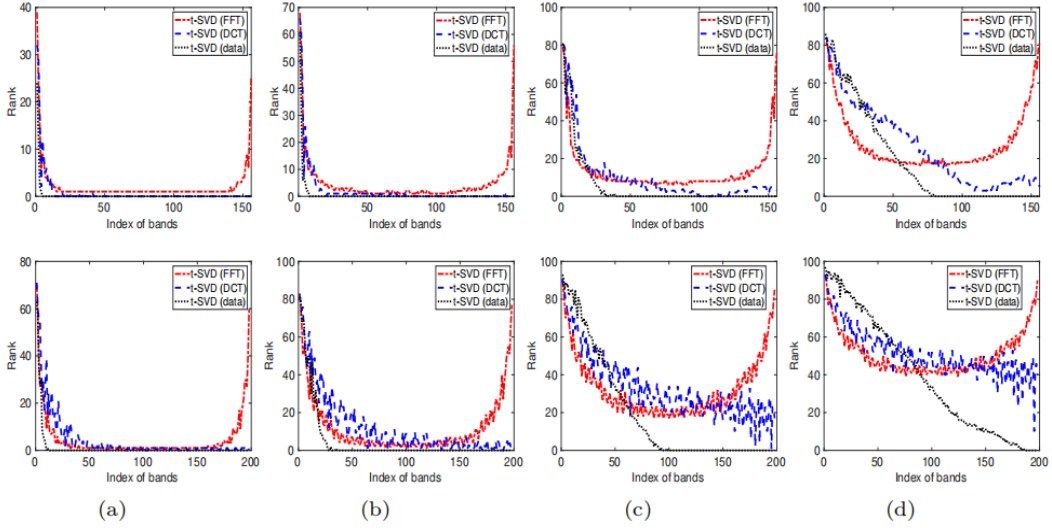


Figure 3: The distribution of transformed multi-ranks of the hyperspectral data sets with different truncations in each band. First row: Samson data set. Second row: Jasper Ridge data set. (a) $\varpi = 70\%$. (b) $\varpi = 80\%$. (c) $\varpi = 90\%$. (d) $\varpi = 95\%$.

Here we compare our method with the low-rank tensor completion method using the sum of nuclear norms of unfolding matrices of a tensor (LRTC)¹ [12, 20], tensor factorization method (TF)² [14], Square Deal [24], gradient descent algorithm on Grassmannians (GoG) [37]. These testing hyperspectral data is normalized on $[0, 1]$. Their theoretical estimation of samples required are presented in Table 1.

We remark that these hyperspectral images are not exactly low multi-rank tensors, the multi-rank $(\sum_{i=1}^{n_3} r_i)$ is not available. A truncated tensor is used to compute the transformed multi-rank and tubal rank by using the threshold ϖ . Here for a given tensor \mathcal{Z} with transformed tensor SVD in (2) of Theorem 2.2 and ϖ , we determine the smallest value k such that

$$\frac{\sum_{i=1}^k \varrho_i}{\sum_{i=1}^{n_{(2)} n_3} \varrho_i} \geq \varpi,$$

where $\{\varrho_i\}$ is the sorted value in ascending order of the numbers $\{(\hat{\mathcal{S}}_{\Phi})_{jj\ell}\}_{1 \leq j \leq n_{(2)}, 1 \leq \ell \leq n_3}$ appearing in the diagonal tensor \mathcal{S} in (2). The ratio is used to determine the significant numbers are kept in the truncated tensor based on the threshold ϖ . Now we can define the transformed multi-rank $\mathbf{r}(\varpi)$ of the truncated tensor as follows:

$$\mathbf{r}(\varpi) := (r_1(\varpi), \dots, r_{n_3}(\varpi)), \text{ with } r_\ell(\varpi) := \#\{(\hat{\mathcal{S}}_{\Phi})_{jj\ell} \geq \varrho_k, 1 \leq j \leq n_{(2)}\}, \ell = 1, \dots, n_3,$$

Accordingly, the transformed tubal rank of the truncated tensor is defined as $r(\varpi) := \max\{r_1(\varpi), \dots, r_{n_3}(\varpi)\}$. The distributions of the transformed multi-ranks of the two hyperspectral data sets with different ϖ are shown in Figure 3. It can be seen that the $\sum_{i=1}^{n_3} r_i(\varpi)$ obtained by t-SVD (data) is much smaller than that obtained by t-SVD (FFT) and t-SVD (DCT) for different truncations $\varpi = 70\%, 80\%, 90\%, 95\%$, which implies that

¹<http://www.cs.rochester.edu/~jliu/>

²<https://homes.cs.washington.edu/~sewoong/papers.html>

Table 2: The PSNR, SSIM values, and CPU time (in seconds) of different methods for the hyper-spectral images.

	const ₁	Samson						
	sampling rate	20	30	40	50	60	70	80
LRTC	PSNR	13.08	16.00	18.34	19.82	20.99	22.12	22.98
	SSIM	0.3254	0.5720	0.6223	0.6643	0.6964	0.7287	0.7548
	CPU	26.44	29.81	29.50	27.13	25.50	26.35	28.66
TF	PSNR	4.05	7.45	20.26	29.78	32.86	35.54	36.39
	SSIM	0.3990	0.4852	0.7798	0.8627	0.8856	0.9334	0.9440
	CPU	207.55	207.20	206.90	206.80	216.99	210.21	207.86
Square Deal	PSNR	16.35	18.55	20.38	22.15	23.77	25.57	26.77
	SSIM	0.4502	0.5727	0.6696	0.7269	0.7916	0.8310	0.8667
	CPU	37.46	34.93	33.05	30.96	29.48	29.63	34.05
GoG	PSNR	16.72	26.02	27.13	30.01	30.45	30.87	31.43
	SSIM	0.4851	0.6978	0.7560	0.8372	0.8366	0.8398	0.8665
	CPU	1.05e4	1.40e4	3.41e4	3.87e4	4.61e4	3.46e4	4.15e4
t-SVD (FFT)	PSNR	22.09	23.88	25.21	26.27	27.09	27.68	28.52
	SSIM	0.5743	0.6498	0.6996	0.7442	0.7689	0.7912	0.8107
	CPU	30.24	26.30	25.11	24.07	22.45	23.62	26.58
t-SVD (DCT)	PSNR	26.35	28.72	30.42	31.92	33.03	33.96	35.04
	SSIM	0.7355	0.8098	0.8552	0.8875	0.9096	0.9215	0.9343
	CPU	172.41	167.56	177.44	185.69	193.36	187.29	190.13
t-SVD (data)	PSNR	28.24	31.37	33.39	35.25	36.53	37.09	38.62
	SSIM	0.8324	0.8971	0.9311	0.9539	0.9643	0.9658	0.9746
	CPU	241.48	258.86	270.17	282.82	284.68	263.78	291.26
	const ₁	Japser Ridge						
	sampling rate	20	30	40	50	60	70	80
LRTC	PSNR	12.48	14.80	16.78	18.17	18.97	19.61	20.15
	SSIM	0.3245	0.4104	0.4404	0.4611	0.4793	0.5011	0.5223
	CPU	39.54	39.98	42.73	39.81	36.51	40.21	42.36
TF	PSNR	7.12	11.41	12.09	15.39	27.03	27.83	28.07
	SSIM	0.2076	0.3728	0.6120	0.6418	0.7246	0.7603	0.7693
	CPU	400.27	399.79	398.94	398.46	286.83	362.15	384.52
Square Deal	PSNR	15.38	17.50	20.47	22.48	24.25	26.13	27.12
	SSIM	0.3890	0.5168	0.6199	0.7021	0.7596	0.8046	0.8378
	CPU	43.33	41.89	41.82	41.99	40.65	42.59	40.99
GoG	PSNR	15.32	22.38	23.54	24.35	25.44	25.90	26.35
	SSIM	0.2643	0.5430	0.5624	0.5835	0.6550	0.6808	0.7193
	CPU	3.49e4	4.13e4	5.33e4	5.50e4	5.58e4	5.39e4	5.41e4
t-SVD (FFT)	PSNR	21.04	22.95	24.09	25.17	26.06	26.74	27.25
	SSIM	0.4877	0.5802	0.6353	0.6891	0.7270	0.7578	0.7756
	CPU	50.54	42.01	37.62	35.38	34.36	42.69	35.99
t-SVD (DCT)	PSNR	21.93	23.40	24.48	25.49	26.36	27.06	27.65
	SSIM	0.5206	0.5945	0.6481	0.7015	0.7378	0.7647	0.7892
	CPU	200.90	171.96	164.15	169.65	172.05	184.23	193.06
t-SVD (data)	PSNR	23.54	25.63	27.47	28.74	30.09	30.78	31.33
	SSIM	0.6004	0.7041	0.7816	0.8323	0.8675	0.8777	0.8962
	CPU	235.74	217.07	217.13	230.64	235.28	225.95	231.87

the t-SVD (data) needs lower number of samples for successful recovery than t-SVD (FFT) and t-SVD (DCT). The distributions of the transformed multi-ranks of the truncated tensor obtained by t-SVD (FFT) are symmetric due to symmetry of FFT.

In Table 2, we present the number of samples ($\text{const}_1 n_{(1)} \log(n_{(1)} n_3)$) for several values of const_1 and their corresponding PSNR and SSIM values of the recovered tensors by different methods, where const_1 varies from 20 to 80 with step-size 10. Here we can regard const_1 as $c_0 \mu \sum_{i=1}^{n_3} r_i(\varpi)$ in (10) of Theorem 3.1. For $\varpi = 70\%$, the values $\sum_{i=1}^{n_3} r_i(\varpi)$ of Samson hyperspectral image are 346, 129, 40 for t-SVD (FFT), t-SVD (DCT), and t-SVD (data), respectively. Thus, the chosen const_1 is proportional to $\sum_{i=1}^{n_3} r_i(\varpi)$ for the testing tensor of hyperspectral image with approximately low transformed multi-rank. We can see from

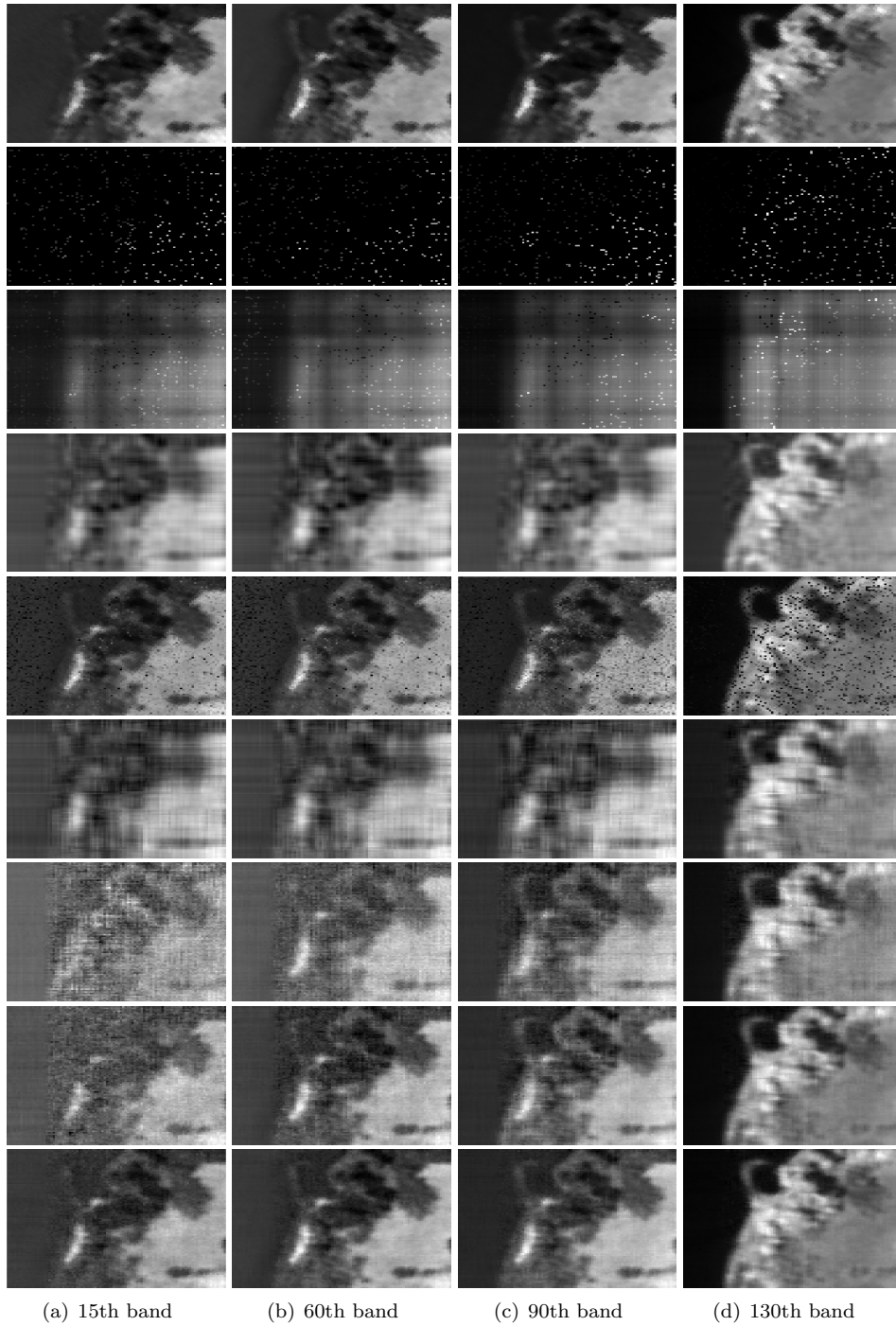


Figure 4: Recovery results by different methods for the Samson data with $\text{const}_1 = 60$. First row: Original images. Second row: Observed images. Third row: Recovered images by LRTC. Fourth row: Recovered images by TF. Fifth row: Recovered images by Square Deal. Sixth row: Recovered images by GoG. Seventh row: Recovered images by t-SVD (FFT). Eighth row: Recovered images by t-SVD (DCT). Ninth row: Recovered images by t-SVD (data).

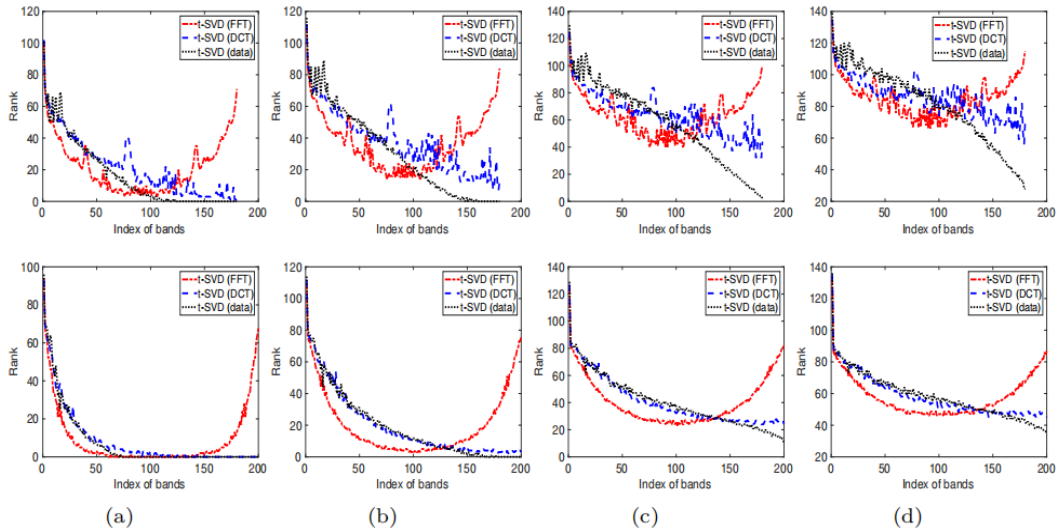


Figure 5: The distribution of transformed multi-ranks of the video data sets with different truncations in each frame. First row: Carphone data set. Second row: Announcer data set. (a) $\varpi = 70\%$. (b) $\varpi = 80\%$. (c) $\varpi = 90\%$. (d) $\varpi = 95\%$.

the table that for different values of const_1 , the PSNR and SSIM values obtained by t-SVD (data) and t-SVD (DCT) are higher than those obtained by LRTC, TF, Square Deal, GoG, and t-SVD (FFT). Moreover, when $\text{const}_1 = 60$, the recovery performance of the t-SVD (FFT), t-SVD (DCT), and t-SVD (data) is good enough in terms of PSNR and SSIM values, which implies the number of sizes is enough for successful recovery by Theorem 3.1. When const_1 is larger, e.g., $\text{const}_1 = 70, 80$, the improvements of PSNR values of the t-SVD (FFT), t-SVD (DCT), and t-SVD (data) are smaller than those of other small const_1 . For Samson data, the performance of GoG is better than that of t-SVD (FFT) for $\text{const}_1 \geq 30$. But the computational time required by GoG is significantly more than that required by the other methods. For Japser Ridge data, the PSNR and SSIM values obtained by all three t-SVD methods are almost higher than those obtained by LRTC, TF, Square Deal, and GoG. Moreover, the computational time required by the t-SVD methods are quite efficient compared with the other methods.

Figure 4 shows the visual comparisons of different bands obtained by LRTC, TF, Square Deal, GoG, and three t-SVD methods for the Samson data, where $\text{const}_1 = 60$. We can see that the t-SVD (data) and t-SVD (DCT) outperform LRTC, TF, Square Deal, and t-SVD (FFT) in terms of visual quality. Moreover, the images recovered by t-SVD (data) keep more details than those recovered by LRTC, TF, Square Deal, t-SVD (FFT), and t-SVD (DCT).

4.2.3 Video Data

In this subsection, we test two video data sets (length \times width \times frames) to show the performance of the proposed method, where the testing videos include Carphone ($144 \times 176 \times 180$) and Announcer ($144 \times 176 \times 200$)³, and we just use the first channels of all frames

³<https://media.xiph.org/video/derf/>

Table 3: The PSNR, SSIM values, and CPU time (in seconds) of different methods for the video data sets.

		const ₁	20	30	40	50	60	70	80	90	100	110	120	
		sampling rate	0.008	0.012	0.016	0.020	0.024	0.028	0.032	0.036	0.040	0.044	0.048	
Carphone	LRTC	PSNR	10.81	11.65	12.49	13.19	13.97	14.75	15.40	16.01	16.53	17.05	17.52	
		SSIM	0.3498	0.3571	0.3687	0.3870	0.4085	0.4319	0.4496	0.4701	0.4862	0.5038	0.5206	
		CPU	90.78	85.06	85.92	85.12	89.76	92.28	91.70	90.47	92.91	92.06	95.21	
	TF	PSNR	4.96	4.64	13.41	12.98	20.82	22.57	22.66	22.74	22.75	22.85	23.04	
		SSIM	0.2855	0.4507	0.5081	0.5499	0.5837	0.6461	0.6531	0.6607	0.6622	0.6705	0.6746	
		CPU	780.55	779.63	771.43	782.11	762.25	770.57	771.03	765.42	760.32	782.45	795.41	
	Square Deal	PSNR	10.04	12.99	13.55	15.00	16.98	17.15	18.10	19.15	20.42	20.47	21.17	
		SSIM	0.1796	0.2675	0.3304	0.3988	0.4497	0.4930	0.5348	0.5719	0.6113	0.6178	0.6396	
		CPU	76.98	80.23	76.06	77.03	76.76	76.36	74.78	80.00	78.59	77.21	79.75	
	GoG	PSNR	18.59	20.18	20.77	20.46	21.22	21.35	21.48	22.11	22.47	22.86	23.15	
		SSIM	0.4010	0.4653	0.5229	0.5023	0.5449	0.5483	0.5547	0.5768	0.5874	0.5936	0.6058	
		CPU	1.09e5	2.27e5	1.30e5	1.40e5	2.47e5	6.27e5	3.76e5	6.71e5	6.32e5	6.52e5	6.48e5	
	t-SVD (FFT)	PSNR	9.79	11.55	15.06	18.53	22.04	22.59	23.07	23.38	23.72	24.01	24.24	
		SSIM	0.1814	0.2463	0.3759	0.4899	0.6121	0.6367	0.6566	0.6690	0.6816	0.6934	0.7017	
		CPU	53.78	58.69	77.43	88.78	107.26	103.15	98.25	93.03	88.88	90.36	92.81	
	t-SVD (DCT)	PSNR	20.24	21.18	21.93	22.42	22.91	23.24	23.60	23.87	24.15	24.44	24.65	
		SSIM	0.5230	0.5720	0.6044	0.6286	0.6506	0.6642	0.6772	0.6890	0.6484	0.7106	0.7185	
		CPU	323.11	291.24	271.55	251.17	237.77	226.54	214.85	205.35	198.58	200.15	197.32	
	t-SVD (data)	PSNR	20.39	21.43	22.30	22.87	23.45	23.75	24.23	24.56	24.85	24.94	25.17	
		SSIM	0.5294	0.5841	0.6236	0.6499	0.6747	0.6877	0.7063	0.7200	0.7298	0.7329	0.7426	
		CPU	366.20	337.21	314.40	293.42	278.06	261.55	253.14	242.91	235.86	261.02	248.59	
			const ₁	20	30	40	50	60	70	80	90	100	110	120
			sampling rate	0.007	0.011	0.015	0.018	0.022	0.025	0.029	0.033	0.036	0.040	0.044
	Announcer	LRTC	PSNR	12.72	14.03	15.28	16.42	17.76	18.83	19.88	20.74	21.46	22.06	22.58
SSIM			0.4727	0.4900	0.5087	0.5336	0.5601	0.5869	0.6120	0.6341	0.6520	0.6710	0.6871	
CPU			100.75	96.25	100.67	103.05	104.02	105.00	104.68	103.02	100.29	101.23	100.96	
TF		PSNR	4.39	9.99	11.36	15.48	24.12	25.65	26.22	26.28	27.99	28.29	28.34	
		SSIM	0.4229	0.6176	0.6599	0.6743	0.7076	0.7363	0.7534	0.7544	0.8169	0.8265	0.8300	
		CPU	887.20	862.11	872.41	874.64	869.01	864.04	822.11	835.96	858.93	862.62	839.15	
Square Deal		PSNR	11.50	14.61	16.71	19.36	20.86	23.34	24.15	24.27	26.76	28.24	28.87	
		SSIM	0.1692	0.2702	0.3780	0.5004	0.6207	0.6950	0.7488	0.7928	0.8394	0.8743	0.8918	
		CPU	86.39	87.33	80.39	78.26	77.23	77.46	80.36	80.28	81.06	80.25	80.38	
GoG		PSNR	21.85	23.59	23.72	24.80	24.96	25.42	26.20	26.87	27.14	27.43	27.79	
		SSIM	0.5113	0.5854	0.6144	0.6691	0.6775	0.6976	0.7183	0.7566	0.7977	0.8236	0.8395	
		CPU	1.94e5	2.31e5	2.60e5	3.54e5	6.09e5	6.36e5	5.49e5	5.98e5	5.90e5	5.89e5	6.01e5	
t-SVD (FFT)		PSNR	11.01	16.64	27.03	27.98	28.63	29.11	29.46	29.83	30.12	30.35	30.62	
		SSIM	0.2606	0.5339	0.8125	0.8380	0.8564	0.8686	0.8776	0.8865	0.8922	0.8987	0.9022	
		CPU	61.87	97.82	153.63	144.82	132.18	125.67	118.75	106.63	103.44	113.25	108.63	
t-SVD (DCT)		PSNR	26.06	27.12	27.92	28.58	29.16	29.58	29.95	30.32	30.69	30.93	31.17	
		SSIM	0.7645	0.8078	0.8353	0.8875	0.8703	0.8798	0.8893	0.8985	0.9046	0.9099	0.9140	
		CPU	537.80	466.05	432.45	407.57	377.23	350.59	329.40	298.93	287.79	298.46	284.32	
t-SVD (data)		PSNR	26.08	27.25	28.12	28.76	29.41	29.88	30.24	30.71	31.14	31.29	31.58	
		SSIM	0.7649	0.8113	0.8399	0.8581	0.8741	0.8838	0.8941	0.9037	0.9106	0.9150	0.9198	
		CPU	608.38	531.39	472.35	460.30	425.59	395.42	353.94	341.43	330.40	365.25	341.29	

in the original data. Moreover, the first 180 and 200 frames for the two videos are chosen to improve the computational time. The intensity range of the video images is scaled into $[0, 1]$ in the experiments.

Similar to Section 4.2.2, the video data sets are not exactly low-rank. First, we show the distributions of the transformed multi-ranks with different transformations and truncations ϖ in Figure 5. It can be observed that the $\sum_{i=1}^{n_3} r_i(\varpi)$ obtained by t-SVD (data) is much smaller than that obtained by t-SVD (FFT) and t-SVD (DCT) for different ϖ . Therefore, the number of samples required by t-SVD (data) would be smaller than that required by t-SVD (FFT) and t-SVD (DCT) for the same performance. The distributions of transformed multi-ranks obtained by t-SVD (FFT) are symmetric for different ϖ since the FFT has symmetric property.

We use $\text{const}_1 n_{(1)} \log(n_{(1)} n_3)$ number of samples based on Theorem 3.1. The range const_1 is from 20 to 120 with increment step-size being 10. For example, when $\varpi = 70\%$, the $\sum_{i=1}^{n_3} r_i(\varpi)$ of Announcer obtained by t-SVD (FFT), t-SVD (DCT), t-SVD (data) are 1886, 1649, 1502, respectively. When const_1 is equal to 100, the required sample size would be enough for successful recovery by Theorem 3.1. When $\text{const}_1 > 100$, e.g., $\text{const}_1 = 110, 120$, the improvements of PSNR values by the three t-SVD methods are very small. In Table 3, we show the PSNR, SSIM values, and CPU time (in seconds) of different methods for the testing video data sets with different const_1 . It can be seen that the performance of t-SVD (data) is better than that of LRTC, TF, Square Deal, GoG, t-SVD (FFT), and t-SVD (DCT)

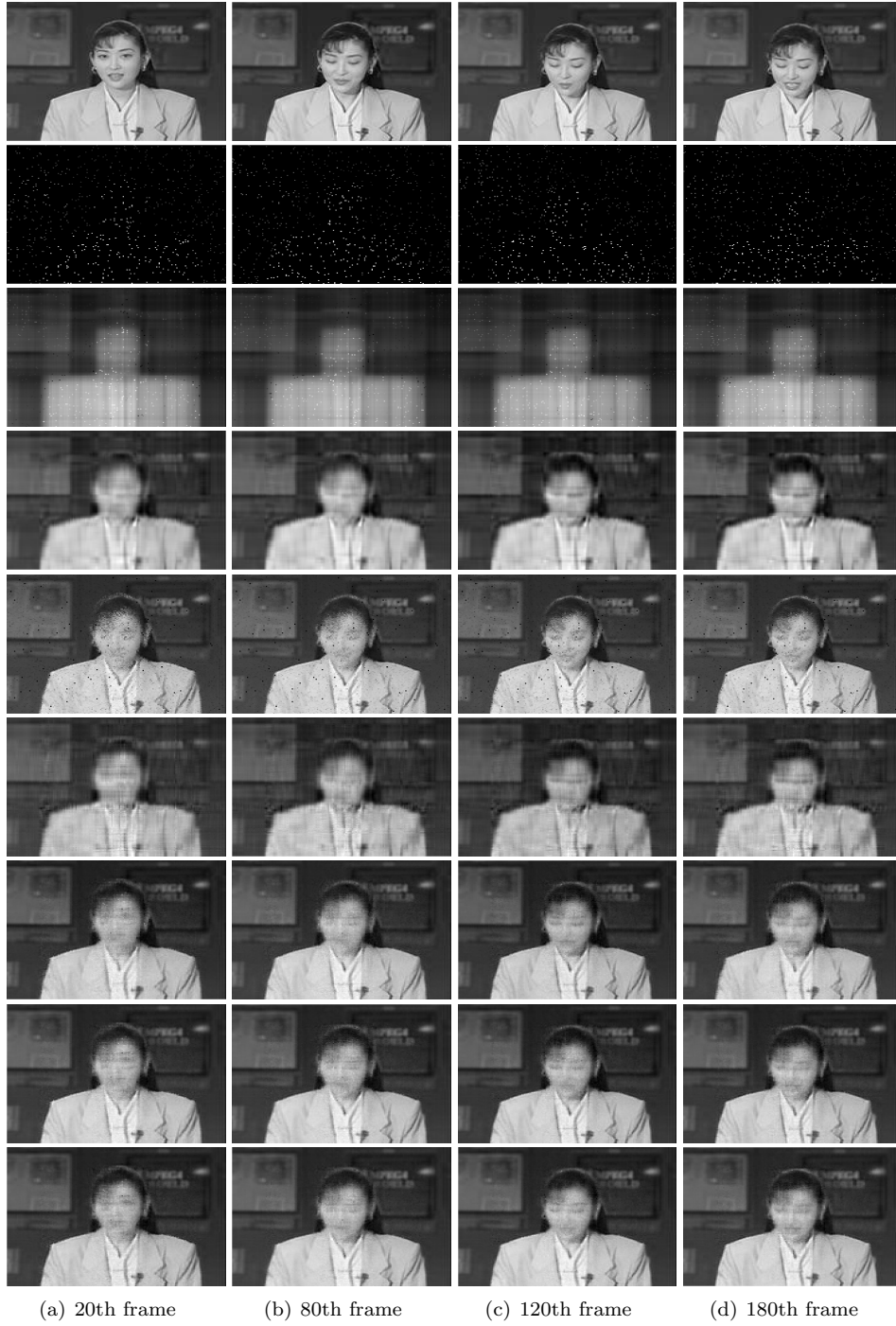


Figure 6: Recovery results by different methods for the Announcer data with $\text{const}_1 = 80$. First row: Original images. Second row: Observed images. Third row: Recovered images by LRTC. Fourth row: Recovered images by TF. Fifth row: Recovered images by Square Deal. Sixth row: Recovered images by GoG. Seventh row: Recovered images by t-SVD (FFT). Eighth row: Recovered images by t-SVD (DCT). Ninth row: Recovered images by t-SVD (data).

in terms of PSNR and SSIM values. The PSNR and SSIM values obtained by t-SVD (DCT) are higher than those obtained by t-SVD (FFT). Hence, the number of samples required by t-SVD (DCT) and t-SVD (data) is smaller than that required by LRTC, TF, Square Deal, GoG, and t-SVD (FFT) for the same recovery performance, which demonstrates the conclusion of Theorem 3.1. Moreover, the CPU time (in seconds) required by GoG is much more than that required by other methods.

Figure 6 shows the visual quality of the 20th, 80th, 120th, 180th frames of the recovered images by LRTC, TF, Square Deal, GoG, and three t-SVD methods, where $\text{const}_1 = 80$. It can be seen that the three t-SVD methods outperform LRTC, TF, Square Deal, and GoG for different frames in terms of visual quality, where the recovered images by the t-SVD methods are more clear.

5 Concluding Remarks

In this paper, we have established the sample size requirement for exact recovery in the tensor completion problem by using transformed tensor SVD. We have shown that for any $\mathcal{Z} \in \mathbb{C}^{n_1 \times n_2 \times n_3}$ with transformed multi-rank $(r_1, r_2, \dots, r_{n_3})$, one can recover the tensor exactly with high probability under some incoherence conditions if the sample size of observations is of the order $O(\sum_{i=1}^{n_3} r_i \max\{n_1, n_2\} \log(\max\{n_1, n_2\} n_3))$ under uniformly sampled entries. The sample size requirement of our theory for exact recovery is smaller than that of existing methods for tensor completion. Moreover, several numerical experiments on both synthetic data and real-world data sets are presented to show the superior performance of our methods in comparison with other state-of-the-art methods.

In further work, it would be of great interest to extend the transformed tensor SVD and tensor completion results to higher-order tensors (cf. [22]). It would be also of great interest to extend the result of the unitary transformation to any invertible linear transformation for tensor completion (cf. [15]).

Acknowledgments

The authors are grateful to Dr. Cun Mu at Walmart Labs and Dr. Dong Xia at The Hong Kong University of Science and Technology for sharing the codes of the Square Deal [24] and GoG methods [37], respectively. The authors are also grateful to the anonymous referees for their constructive suggestions and comments to improve the presentation of the paper.

Appendix A.

We first list the following lemma, which is the main tool to prove our conclusions.

Lemma 5.1. (*[28, Theorem 4]*) *Let $X_1, \dots, X_L \in \mathbb{R}^{n \times n}$ be independent zero mean random matrices of dimension $d_1 \times d_2$. Suppose $\rho_k^2 = \max\{\|\mathbb{E}[X_k X_k^T]\|, \|\mathbb{E}[X_k^T X_k]\|\}$ and $\|X_k\| \leq B$ almost surely for all $k = 1, \dots, L$. Then for any $\tau > 0$,*

$$\mathbb{P} \left[\left\| \sum_{k=1}^L X_k \right\| > \tau \right] \leq (d_1 + d_2) \exp \left(\frac{-\tau^2/2}{\sum_{k=1}^L \rho_k^2 + B\tau/3} \right).$$

Moreover, if $\max \left\{ \left\| \sum_{k=1}^L X_k X_k^T \right\|, \left\| \sum_{k=1}^L X_k^T X_k \right\| \right\} \leq \sigma^2$, then for any $c > 1$, we have

$$\left\| \sum_{k=1}^L X_k \right\| \leq \sqrt{4c\sigma^2 \log(d_1 + d_2)} + cB \log(d_1 + d_2)$$

holds with probability at least $1 - (d_1 + d_2)^{-(c-1)}$.

Proof of Lemma 3.3

Let \mathcal{E}_{ijk} be a unit tensor whose (i, j, k) -th entry is 1 and others are 0. Then for an arbitrary tensor $\mathcal{Z} \in \mathbb{C}^{n_1 \times n_2 \times n_3}$, we have $\mathcal{Z} = \sum_{i,j,k} \langle \mathcal{E}_{ijk}, \mathcal{Z} \rangle \mathcal{E}_{ijk}$. Recall Definition 2.7, \mathcal{E}_{ijk} can be expressed as $\mathcal{E}_{ijk} = \vec{e}_{ik} \diamond_{\Phi} \check{e}_k \diamond_{\Phi} \vec{e}_{jk}^H$, then $\mathcal{P}_T(\mathcal{Z})$ can also be decomposed as

$$\mathcal{P}_T(\mathcal{Z}) = \sum_{i,j,k} \langle \mathcal{P}_T(\mathcal{Z}), \vec{e}_{ik} \diamond_{\Phi} \check{e}_k \diamond_{\Phi} \vec{e}_{jk}^H \rangle \vec{e}_{ik} \diamond_{\Phi} \check{e}_k \diamond_{\Phi} \vec{e}_{jk}^H,$$

where T is defined as (9). Similarly,

$$\rho^{-1} \mathcal{P}_T \mathcal{P}_{\Omega} \mathcal{P}_T(\mathcal{Z}) = \sum_{i,j,k} \rho^{-1} \delta_{ijk} \langle \mathcal{Z}, \mathcal{P}_T(\vec{e}_{ik} \diamond_{\Phi} \check{e}_k \diamond_{\Phi} \vec{e}_{jk}^H) \rangle \mathcal{P}_T(\vec{e}_{ik} \diamond_{\Phi} \check{e}_k \diamond_{\Phi} \vec{e}_{jk}^H).$$

Define the operator \mathcal{T}^{ijk} as:

$$\mathcal{T}^{ijk}(\mathcal{Z}) = \rho^{-1} \delta_{ijk} \langle \mathcal{Z}, \mathcal{P}_T(\vec{e}_{ik} \diamond_{\Phi} \check{e}_k \diamond_{\Phi} \vec{e}_{jk}^H) \rangle \mathcal{P}_T(\vec{e}_{ik} \diamond_{\Phi} \check{e}_k \diamond_{\Phi} \vec{e}_{jk}^H).$$

Then by the definition of tensor operator norm, we can get

$$\|\mathcal{T}^{ijk}\|_{\text{op}} = \frac{1}{\rho} \|\mathcal{P}_T(\vec{e}_{ik} \diamond_{\Phi} \check{e}_k \diamond_{\Phi} \vec{e}_{jk}^H)\|_F^2, \text{ and } \|\mathcal{P}_T\|_{\text{op}} \leq 1.$$

Note the fact that for any two positive semidefinite matrices $A, B \in \mathbb{C}^{n \times n}$, we have $\|A - B\| \leq \max\{\|A\|, \|B\|\}$. Therefore, by the inequality given in Proposition 3.2, we have

$$\left\| \mathcal{T}^{ijk} - \frac{1}{n_1 n_2 n_3} \mathcal{P}_T \right\|_{\text{op}} \leq \max \left\{ \frac{1}{\rho} \|\mathcal{P}_T(\vec{e}_{ik} \diamond_{\Phi} \check{e}_k \diamond_{\Phi} \vec{e}_{jk}^H)\|_F^2, \frac{1}{n_1 n_2 n_3} \right\} \leq \frac{2\mu \sum r_i}{n_{(2)} n_3 \rho}.$$

In addition, one has

$$\begin{aligned} & \left\| \mathbb{E} \left(\mathcal{T}^{ijk} - \frac{1}{n_1 n_2 n_3} \mathcal{P}_T \right) \right\|_{\text{op}} \\ & \leq \left\| \mathbb{E} \left(\frac{1}{\rho} \|\mathcal{P}_T(\vec{e}_{ik} \diamond_{\Phi} \check{e}_k \diamond_{\Phi} \vec{e}_{jk}^H)\|_F^2 \mathcal{T}^{ijk} \right) - \frac{2}{n_1 n_2 n_3} \mathcal{P}_T \mathbb{E}(\mathcal{T}^{ijk}) + \frac{1}{n_1^2 n_2^2 n_3^2} \mathcal{P}_T \right\| \\ & = \left\| \frac{1}{\rho} \|\mathcal{P}_T(\vec{e}_{ik} \diamond_{\Phi} \check{e}_k \diamond_{\Phi} \vec{e}_{jk}^H)\|_F^2 \frac{1}{n_1 n_2 n_3} \mathcal{P}_T - \frac{1}{n_1^2 n_2^2 n_3^2} \mathcal{P}_T \right\| \leq \frac{2\mu \sum r_i}{n_{(1)} n_{(2)}^2 n_3^2 \rho}. \end{aligned}$$

Setting $\tau = \sqrt{\frac{14\mu\beta \sum r_i \log(n_{(1)} n_3)}{3n_{(2)} n_3 \rho}} \leq \frac{1}{2}$ with any $\beta > 1$ and using Lemma 5.1, we have

$$\begin{aligned} & \mathbb{P}[\|\rho^{-1} \mathcal{P}_T \mathcal{P}_{\Omega} \mathcal{P}_T - \mathcal{P}_T\|_{\text{op}} > \tau] = \mathbb{P} \left[\left\| \sum_{i,j,k} \left(\mathcal{T}^{ijk} - \frac{1}{n_1 n_2 n_3} \mathcal{P}_T \right) \right\|_{\text{op}} > \tau \right] \\ & \leq 2n_{(1)} n_3 \exp \left(\frac{-7\mu\beta \sum r_i \log(n_{(1)} n_3)}{3n_{(2)} n_3 \rho} \right) = 2n_{(1)} n_3 \exp(-\beta \log n_{(1)} n_3) = 2(n_{(1)} n_3)^{1-\beta}, \end{aligned}$$

which implies that

$$\mathbb{P} \left[\|\rho^{-1} \mathcal{P}_T \mathcal{P}_\Omega \mathcal{P}_T - \mathcal{P}_T\|_{\text{op}} \leq \epsilon \right] \geq 1 - 2(n_{(1)} n_3)^{1-\beta}.$$

This completes the proof.

Appendix B. Proof of Lemma 3.4

Denote

$$\rho^{-1} \mathcal{P}_\Omega(\mathcal{Z}) - \mathcal{Z} = \sum_{i,j,k} \mathcal{G}^{ijk} = \sum_{i,j,k} \left(\frac{1}{\rho} \delta_{ijk} - 1 \right) \mathcal{Z}_{ijk} \vec{e}_{ik} \diamond_{\Phi} \vec{e}_k \diamond_{\Phi} \vec{e}_{jk}^H.$$

Then by the independence of δ_{ijk} , we have $\mathbb{E}[\mathcal{G}^{ijk}] = \mathbf{0}$ and $\|\mathcal{G}^{ijk}\| \leq \frac{1}{\rho} \|\mathcal{Z}\|_{\infty}$. Moreover,

$$\begin{aligned} \left\| \mathbb{E} \left[\sum_{i,j,k} (\mathcal{G}^{ijk})^H \diamond_{\Phi} \mathcal{G}^{ijk} \right] \right\| &= \left\| \sum_{i,j,k} |\mathcal{Z}_{ijk}|^2 \vec{e}_{jk} \diamond_{\Phi} \vec{e}_{jk}^H \mathbb{E} \left(\frac{1}{\rho} \delta_{ijk} - 1 \right)^2 \right\| \\ &= \left\| \frac{1-\rho}{\rho} \sum_{i,j,k} |\mathcal{Z}_{ijk}|^2 \vec{e}_{ik} \diamond_{\Phi} \vec{e}_{ik}^H \right\|. \end{aligned}$$

Recall the definition of tensor basis, we can get that $\Phi[\vec{e}_{jk} \diamond_{\Phi} \vec{e}_{jk}^H]$ is a tensor except the (j, j, t) -th tube entries equaling to $(\Phi[\vec{e}_k]_t)^2 = \alpha_t^2, t = 1, \dots, n_3$ with $\sum_{t=1}^{n_3} \alpha_t^2 = 1$, and 0 otherwise. Hence, we get that

$$\begin{aligned} \left\| \mathbb{E} \left[\sum_{i,j,k} (\mathcal{G}^{ijk})^H \diamond_{\Phi} \mathcal{G}^{ijk} \right] \right\| &= \frac{1-\rho}{\rho} \left\| \sum_{i,j,k} |\mathcal{Z}_{ijk}|^2 \vec{e}_{jk} \diamond_{\Phi} \vec{e}_{jk}^H \right\| \\ &= \frac{1-\rho}{\rho} \max_j \left\| \sum_{i,j,k} |\mathcal{Z}_{ijk}|^2 \vec{e}_{jk} \diamond_{\Phi} \vec{e}_{jk}^H \right\| \\ &= \frac{1-\rho}{\rho} \max_j \left\| \sum_{i,k} |\mathcal{Z}_{ijk}|^2 (\vec{e}_{jk})_{\Phi} \cdot (\vec{e}_{jk})_{\Phi}^H \right\| \leq \frac{1}{\rho} \|\mathcal{Z}\|_{\infty, w}^2. \end{aligned}$$

Moreover, $\left\| \mathbb{E} \left[\sum_{i,j,k} \mathcal{G}^{ijk} \diamond_{\Phi} (\mathcal{G}^{ijk})^H \right] \right\|$ can be also bounded similarly. Then by Lemma 5.1, we can get that

$$\|\rho^{-1} \mathcal{P}_\Omega(\mathcal{Z}) - \mathcal{Z}\|_{\text{op}} \leq c \left(\frac{\log(n_{(1)} n_3)}{\rho} \|\mathcal{Z}\|_{\infty} + \sqrt{\frac{\log(n_{(1)} n_3)}{\rho}} \|\mathcal{Z}\|_{\infty, w} \right)$$

holds with high probability provided that $m \geq C_0 \epsilon^{-2} \mu \sum r_i n_{(1)} \log(n_{(1)} n_3)$.

Appendix C. Proof of Lemma 3.5

Denote the weighted b -th lateral slice of $(\rho^{-1}\mathcal{P}_T\mathcal{P}_\Omega - \mathcal{P}_T)\mathcal{Z}$ as

$$\begin{aligned}\sum_{i,j,k} \mathcal{F}^{ijk} &:= (\rho^{-1}\mathcal{P}_T\mathcal{P}_\Omega - \mathcal{P}_T)\mathcal{Z} \diamond_{\Phi} \vec{e}_{bk} \\ &= \sum_{i,j,k} \left(\frac{1}{\rho} \delta_{ijk} - 1 \right) \mathcal{Z}_{ijk} \mathcal{P}_T(\vec{e}_{ik} \diamond_{\Phi} \dot{e}_k \diamond_{\Phi} \vec{e}_{jk}^H) \diamond_{\Phi} \vec{e}_{bk},\end{aligned}$$

where $\mathcal{F}^{ijk} \in \mathbb{C}^{n_1 \times 1 \times n_3}$ are zero-mean independent lateral slices. By the incoherence conditions given in Proposition 3.2, we have

$$\|\mathcal{F}^{ijk}\|_F = \left\| \left(\frac{1}{\rho} \delta_{ijk} - 1 \right) \mathcal{Z}_{ijk} \mathcal{P}_T(\vec{e}_{ik} \diamond_{\Phi} \dot{e}_k \diamond_{\Phi} \vec{e}_{jk}^H) \diamond_{\Phi} \vec{e}_{bk} \right\|_F \leq \frac{1}{\rho} \sqrt{\frac{2\mu \sum_{i=1}^{n_3} r_i}{n_1 n_3}} \|\mathcal{Z}\|_{\infty}.$$

Furthermore,

$$\left\| \mathbb{E} \left[\sum_{i,j,k} (\mathcal{F}^{ijk})^H \diamond_{\Phi} \mathcal{F}^{ijk} \right] \right\|_F = \frac{1-\rho}{\rho} \sum_{i,j,k} |\mathcal{Z}_{ijk}|^2 \|\mathcal{P}_T(\vec{e}_{ik} \diamond_{\Phi} \dot{e}_k \diamond_{\Phi} \vec{e}_{jk}^H) \diamond_{\Phi} \vec{e}_{bk}\|_F^2.$$

Then by the definition of \mathcal{P}_T , we can get

$$\begin{aligned}& \|\mathcal{P}_T(\vec{e}_{ik} \diamond_{\Phi} \dot{e}_k \diamond_{\Phi} \vec{e}_{jk}^H) \diamond_{\Phi} \vec{e}_{bk}\|_F^2 \\ &= \|\mathcal{U} \diamond_{\Phi} \mathcal{U}^H \diamond_{\Phi} \vec{e}_{ik} \diamond_{\Phi} \dot{e}_k \diamond_{\Phi} \vec{e}_{jk}^H \diamond_{\Phi} \vec{e}_{bk}\|_F^2 \\ & \quad + \|\mathcal{I}_{\Phi} - \mathcal{U} \diamond_{\Phi} \mathcal{U}^H\|_F \|\vec{e}_{ik} \diamond_{\Phi} \dot{e}_k \diamond_{\Phi} \vec{e}_{jk}^H \diamond_{\Phi} \mathcal{V} \diamond_{\Phi} \mathcal{V}^H \diamond_{\Phi} \vec{e}_{bk}\|_F^2 \\ &\leq \frac{\mu \sum_{i=1}^{n_3} r_i}{n_1 n_3} \|\dot{e}_k \diamond_{\Phi} \vec{e}_{jk} \diamond_{\Phi} \vec{e}_{bk}\|_F^2 + \|\vec{e}_{jk}^H \diamond_{\Phi} \mathcal{V} \diamond_{\Phi} \mathcal{V}^H \diamond_{\Phi} \vec{e}_{bk}\|_F^2.\end{aligned}$$

Therefore, we obtain

$$\begin{aligned}& \left\| \mathbb{E} \left[\sum_{i,j,k} (\mathcal{F}^{ijk})^H \diamond_{\Phi} \mathcal{F}^{ijk} \right] \right\|_F \\ &\leq \frac{1}{\rho} \sum_{i,j,k} |\mathcal{Z}_{ijk}|^2 \|\mathcal{P}_T(\vec{e}_{ik} \diamond_{\Phi} \dot{e}_k \diamond_{\Phi} \vec{e}_{jk}^H) \diamond_{\Phi} \vec{e}_{bk}\|_F^2 \\ &\leq \frac{1}{\rho} \sum_{i,j,k} |\mathcal{Z}_{ijk}|^2 \frac{\mu \sum_{i=1}^{n_3} r_i}{n_1 n_3} \|\dot{e}_k \diamond_{\Phi} \vec{e}_{jk} \diamond_{\Phi} \vec{e}_{bk}\|_F^2 + \frac{1}{\rho} \sum_{i,j,k} |\mathcal{Z}_{ijk}|^2 \|\vec{e}_{jk}^H \diamond_{\Phi} \mathcal{V} \diamond_{\Phi} \mathcal{V}^H \diamond_{\Phi} \vec{e}_{bk}\|_F^2 \\ &\leq \frac{\mu \sum_{i=1}^{n_3} r_i}{\rho n_1 n_3} \|\mathcal{Z}\|_{\infty, w}^2 + \frac{1}{\rho} \sum_{i,k} |\mathcal{Z}_{ijk}|^2 \|\vec{e}_{jk}^H \diamond_{\Phi} \mathcal{V} \diamond_{\Phi} \mathcal{V}^H \diamond_{\Phi} \vec{e}_{bk}\|_F^2 \\ &\leq \frac{2\mu \sum_{i=1}^{n_3} r_i}{\rho n_{(2)} n_3} \|\mathcal{Z}\|_{\infty, w}^2,\end{aligned}$$

where the third inequality can be derived by $\vec{e}_{jk}^H \diamond_{\Phi} \vec{e}_{bk} = \mathbf{0}$ if $j \neq b$. By the same argument, $\left\| \mathbb{E}[\sum_{i,j,k} \mathcal{F}^{ijk} \diamond_{\Phi} (\mathcal{F}^{ijk})^H] \right\|_F$ can be bounded by the same quantity. Therefore, by Lemma 5.1, we get that

$$\|(\rho^{-1}\mathcal{P}_T\mathcal{P}_\Omega - \mathcal{P}_T)\mathcal{Z} \diamond_{\Phi} \vec{e}_{bk}\|_F \leq \frac{1}{2} \|\mathcal{Z}\|_{\infty, w} + \frac{1}{2} \sqrt{\frac{n_{(1)} n_3}{\mu \sum_{i=1}^{n_3} r_i}} \|\mathcal{Z}\|_{\infty}$$

holds with high probability. We can also get the same results with respect to $\bar{\mathbf{e}}_{ak}^H \diamond_{\Phi}$ $(\rho^{-1}\mathcal{P}_T\mathcal{P}_\Omega - \mathcal{P}_T)\mathcal{Z}$. Then Lemma 3.5 follows from using a union bound over all the tensor columns and rows, and the desired results hold with high probability.

References

- [1] T. Ahmed, H. Raja, and W. U. Bajwa. Tensor regression using low-rank and sparse Tucker decompositions. *SIAM Journal on Mathematics of Data Science*, 2(4):944–966, 2020.
- [2] B. Barak and A. Moitra. Noisy tensor completion via the sum-of-squares hierarchy. In *Conference on Learning Theory*, pages 417–445, 2016.
- [3] J.-F. Cai, L. Miao, Y. Wang, and Y. Xian. Provable near-optimal low-multilinear-rank tensor recovery. *arXiv:2007.08904*, 2020.
- [4] E. J. Candès, X. Li, Y. Ma, and J. Wright. Robust principal component analysis? *Journal of the ACM*, 58(3):11, 2011.
- [5] E. J. Candès and Y. Plan. Matrix completion with noise. *Proceedings of the IEEE*, 98(6):925–936, 2010.
- [6] E. J. Candès and B. Recht. Exact matrix completion via convex optimization. *Foundations of Computational Mathematics*, 9(6):717–772, 2009.
- [7] E. J. Candès and T. Tao. The power of convex relaxation: Near-optimal matrix completion. *IEEE Transactions on Information Theory*, 56(5):2053–2080, 2010.
- [8] Y. Chen. Incoherence-optimal matrix completion. *IEEE Transactions on Information Theory*, 61(5):2909–2923, 2015.
- [9] M. Fazel, T. K. Pong, D. Sun, and P. Tseng. Hankel matrix rank minimization with applications to system identification and realization. *SIAM Journal on Matrix Analysis and Applications*, 34(3):946–977, 2013.
- [10] R. Glowinski and A. Marroco. Sur l’approximation, par éléments finis d’ordre un, et la résolution, par pénalisation-dualité d’une classe de problèmes de Dirichlet non linéaires. *Revue Française d’Automatique Informatique, Recherche Opérationnelle. Analyse Numérique*, 9(R2):41–76, 1975.
- [11] D. Gross. Recovering low-rank matrices from few coefficients in any basis. *IEEE Transactions on Information Theory*, 57(3):1548–1566, 2011.
- [12] B. Huang, C. Mu, D. Goldfarb, and J. Wright. Provable models for robust low-rank tensor completion. *Pacific Journal of Optimization*, 11(2):339–364, 2015.
- [13] T. Imbiriba, R. A. Borsoi, and J. C. M. Bermudez. A low-rank tensor regularization strategy for hyperspectral unmixing. In *2018 IEEE Statistical Signal Processing Workshop (SSP)*, pages 373–377. IEEE, 2018.
- [14] P. Jain and S. Oh. Provable tensor factorization with missing data. In *Advances in Neural Information Processing Systems*, pages 1431–1439, 2014.

- [15] E. Kernfeld, M. Kilmer, and S. Aeron. Tensor-tensor products with invertible linear transforms. *Linear Algebra and its Applications*, 485:545–570, 2015.
- [16] M. E. Kilmer, K. Braman, N. Hao, and R. C. Hoover. Third-order tensors as operators on matrices: A theoretical and computational framework with applications in imaging. *SIAM Journal on Matrix Analysis and Applications*, 34(1):148–172, 2013.
- [17] M. E. Kilmer and C. D. Martin. Factorization strategies for third-order tensors. *Linear Algebra and its Applications*, 435(3):641–658, 2011.
- [18] T. G. Kolda and B. W. Bader. Tensor decompositions and applications. *SIAM Review*, 51(3):455–500, 2009.
- [19] A. Krishnamurthy and A. Singh. Low-rank matrix and tensor completion via adaptive sampling. In *Advances in Neural Information Processing Systems*, pages 836–844, 2013.
- [20] J. Liu, P. Musialski, P. Wonka, and J. Ye. Tensor completion for estimating missing values in visual data. *IEEE Transactions on Pattern Analysis and Machine Intelligence*, 35(1):208–220, 2013.
- [21] Y. Luo and A. R. Zhang. Low-rank tensor estimation via Riemannian Gauss-Newton: Statistical optimality and second-order convergence. *arXiv:2104.12031*, 2021.
- [22] C. D. Martin, R. Shafer, and B. LaRue. An order-p tensor factorization with applications in imaging. *SIAM Journal on Scientific Computing*, 35(1):A474–A490, 2013.
- [23] A. Montanari and N. Sun. Spectral algorithms for tensor completion. *Communications on Pure and Applied Mathematics*, 71(11):2381–2425, 2018.
- [24] C. Mu, B. Huang, J. Wright, and D. Goldfarb. Square deal: Lower bounds and improved relaxations for tensor recovery. In *International Conference on Machine Learning*, pages 73–81, 2014.
- [25] M. K. Ng, Q. Yuan, L. Yan, and J. Sun. An adaptive weighted tensor completion method for the recovery of remote sensing images with missing data. *IEEE Transactions on Geoscience and Remote Sensing*, 55(6):3367–3381, 2017.
- [26] D. Qiu, M. Bai, M. K. Ng, and X. Zhang. Nonlocal robust tensor recovery with non-convex regularization. *Inverse Problems*, 37(3):035001, 2021.
- [27] H. Rauhut, R. Schneider, and Ž. Stojanac. Low rank tensor recovery via iterative hard thresholding. *Linear Algebra and its Applications*, 523:220–262, 2017.
- [28] B. Recht. A simpler approach to matrix completion. *Journal of Machine Learning Research*, 12:3413–3430, 2011.
- [29] B. Recht, M. Fazel, and P. A. Parrilo. Guaranteed minimum-rank solutions of linear matrix equations via nuclear norm minimization. *SIAM Review*, 52(3):471–501, 2010.
- [30] B. Romera-Paredes, H. Aung, N. Bianchi-Berthouze, and M. Pontil. Multilinear multitask learning. In *International Conference on Machine Learning*, pages 1444–1452, 2013.
- [31] M. Signoretto, Q. T. Dinh, L. De Lathauwer, and J. A. Suykens. Learning with tensors: a framework based on convex optimization and spectral regularization. *Machine Learning*, 94(3):303–351, 2014.

- [32] G. Song, M. K. Ng, and X. Zhang. Robust tensor completion using transformed tensor singular value decomposition. *Numerical Linear Algebra with Applications*, 27(3):e2299, 2020.
- [33] R. Tomioka, T. Suzuki, K. Hayashi, and H. Kashima. Statistical performance of convex tensor decomposition. In *Advances in Neural Information Processing Systems*, pages 972–980, 2011.
- [34] T. Tong, C. Ma, A. Prater-Bennette, E. Tripp, and Y. Chi. Scaling and scalability: Provable nonconvex low-rank tensor estimation from incomplete measurements. *arXiv:2104.14526*, 2021.
- [35] L. R. Tucker. Some mathematical notes on three-mode factor analysis. *Psychometrika*, 31(3):279–311, 1966.
- [36] Z. Wang, A. C. Bovik, H. R. Sheikh, and E. P. Simoncelli. Image quality assessment: From error visibility to structural similarity. *IEEE Transactions on Image Processing*, 13(4):600–612, 2004.
- [37] D. Xia and M. Yuan. On polynomial time methods for exact low rank tensor completion. *Foundations of Computational Mathematics*, 19(6):1265–1313, 2019.
- [38] M. Yuan and C.-H. Zhang. On tensor completion via nuclear norm minimization. *Foundations of Computational Mathematics*, 16(4):1031–1068, 2016.
- [39] M. Yuan and C.-H. Zhang. Incoherent tensor norms and their applications in higher order tensor completion. *IEEE Transactions on Information Theory*, 63(10):6753–6766, 2017.
- [40] X. Zhang and M. K. Ng. A corrected tensor nuclear norm minimization method for noisy low-rank tensor completion. *SIAM Journal on Imaging Sciences*, 12(2):1231–1273, 2019.
- [41] X. Zhang and M. K.-P. Ng. Low rank tensor completion with Poisson observations. *IEEE Transactions on Pattern Analysis and Machine Intelligence*, DOI: 10.1109/TPAMI.2021.3059299, 2021.
- [42] Z. Zhang and S. Aeron. Exact tensor completion using t-SVD. *IEEE Transactions on Signal Processing*, 65(6):1511–1526, 2017.
- [43] F. Zhu, Y. Wang, B. Fan, S. Xiang, G. Meng, and C. Pan. Spectral unmixing via data-guided sparsity. *IEEE Transactions on Image Processing*, 23(12):5412–5427, 2014.